

UC Berkeley

UC Berkeley Electronic Theses and Dissertations

Title

Laser Assisted Direct Local Synthesis of Semiconducting Nanowires

Permalink

<https://escholarship.org/uc/item/2912b8f0>

Author

RYU, SANG GIL

Publication Date

2010

Peer reviewed|Thesis/dissertation

Laser Assisted Direct Local Synthesis of Semiconducting Nanowires

By

Sang Gil Ryu

A dissertation submitted in partial satisfaction of the

requirements for the degree of

Doctor of Philosophy

in

Engineering-Mechanical Engineering

in the

Graduate Division

of the

University of California, Berkeley

Committee in charge:

Professor Costas P. Grigoropoulos, Chair

Professor Van P. Carey

Professor Andrew Minor

Fall 2010

Laser Assisted Direct Local Synthesis of Semiconducting Nanowires

Copyright © 2010

By

Sang Gil Ryu

Abstract

Laser Assisted Direct Local Synthesis of Semiconducting Nanowires

by

Sang Gil Ryu

Doctor of Philosophy in Engineering-Mechanical Engineering

University of California, Berkeley

Professor Costas P. Grigoropoulos, Chair

Semiconductor nanowires have been in the spotlight, carrying great promise for realization of future generation devices spanning diverse fields including electronics and photonics, biotechnology, and energy conversion and storage. In order to realize these functionalities, new techniques must be developed that will enable the precise layout and assembly of the homogenous or heterogeneous components into functional superblocks. This thesis puts forward laser assisted direct localized growth as a promising route for the synthesis of semiconductor nanowires that has been previously hard to achieve.

Laser has been considered as a versatile and efficient tool for micro- and nano-structure fabrication for several decades. By taking advantage of rapid and spatially confined heating capabilities of laser radiation, nanostructures can be synthesized only within a confined high temperature region over the threshold processing temperature. The surroundings structure hence remains at room temperature, allowing minimization of damage of various device components that lie on the wafer platform. In addition, via the direct synthesis capability, nanoscale materials can be grown with an arbitrary position accuracy.

In this study, laser assisted silicon nanowire (SiNW) growth is explored using assembled gold nanoparticles (AuNPs) on the silicon thin film. Continuous wave (CW) laser illumination is employed of 514 nm wavelength and different laser illumination direction. Parametric study is carried out by controlling the process conditions such as growth time, laser power, and laser illumination direction, which demonstrates the advantage of laser-assisted process. Film-side illumination is favorable for localized heating within the catalysts through plasmonic resonance and allows one-dimensional (1-D) nanowire growth at very early stage. However, subsequent growth is dominated

by secondary silicon deposition on the pre-grown portion of nanowires. On the contrary, substrate-side illumination enabling indirect heating of the catalysts through the light absorbing layer of amorphous silicon film thicker than the optical penetration depth of the laser radiation leads to stable and controlled growth of silicon nanowires. Although kinetic analysis confirms that the growth behavior follows the usual Arrhenius growth trend, it is shown that the growth rate of laser-assisted silicon nanowires is faster than in conventional furnace based growth possibly due to three-dimensional diffusion of reactant gases into the localized hot spot.

Motivated by the fast localized heating capability of laser enabling high temporal resolution, a detailed investigation is carried out on the mechanism of laser assisted growth of SiNWs such as diameter- and temperature-dependence of nucleation and catalyst diameter dependence of activation energy of the diffusion of silicon through solid Au. From this investigation, it is confirmed that laser-assisted technique comprises a systematic tool to explore nano-synthesized materials.

To realize SiNWs-based devices, it is also important to grow them with controlled direction, and arrange, or assemble as-grown SiNWs on existing device. However, most techniques to date face problems with their low yield or insufficient spatial resolution. In this study, two fabrication methods are proposed that are more favorable for direct fabrication of semiconducting nanowires on prescribed devices without post-process such as alignment and assembly. One is to employ an optical near-field probe coupled with a laser. Confined beam beyond the diffraction limit by employing optical near-field probes enabling nanoscale heating source realizes the growth of a single SiNW from a specific catalyst particle among the randomly distributed and separated by nanometric distances AuNPs on the substrate. The other is to employ an electrically biased sharp tip, which is more focused on the controlled growth of a SiNW as well as highly selective growth. It is demonstrated that a short SiNW can be grown and aligned along the direction of the induced electric field by pulling the catalyst (AuNP) along the same direction thanks to strongly enhanced electrostatic force by a biased sharp tip. The electrostatic force is also examined as a driving force by a biased sharp tip. As a calibration step, the deflection of the tip with respect to applied bias voltage is measured and the force is quantified by Hook's law.

Dedicated to my wife, Hyojin Choi, and our parents

ACKNOWLEDGEMENTS

First of all, I would like to express sincere gratitude to my research adviser, Professor Costas P. Grigoropoulos, for his guidance, encouraging advice, and financial support. Without his advice and guidance, I would never have reached this point in my research. He has been more than an advisor; his vision, inspiration, and enthusiasm will guide me throughout my life. His enthusiasm and sense of humor even in unrelenting durations of unsuccessful experiments made it easier to keep moving ahead in my research.

I would like to give my thanks to Professor Oscar Dubon of the Department of Material Science and Engineering for insightful discussions and invaluable advice on my research. I know he guided me to the right path with sincerity. I am also thankful to Professor Van P. Carey of the Department of Mechanical Engineering and Professor Andrew Minor of the Department of Material Science and Engineering for taking time out from their busy schedules to be on my qualifying examination committee and dissertation committee.

It has been a great pleasure to work together with Dr. David J. Hwang in Laser Thermal Lab. I wouldn't have reached this point without his all invaluable discussions and helps. I am extremely thankful to him for being my good mentor as well as coworker in my research. He deserves my warmhearted gratitude. I would also like to thank all previous and current members in LTL during my research for their support and help: Dr. Hyung-gyu Park, Dr. Seunghwan Ko, Dr. Matthew Rogers, Dr. Moosung Kim, Dr. Ming-Tsang Lee, Dr. Nipun Misra, Dr. Heng Pan, Hojeong Jeon, Jungbin In, Travis Owens, Kyounghoon Kim, Daeho Lee, Sanghoon Ahn, Eunpa Kim.

Finally, my efforts would not have been successful without the love, blessing and understanding of my parents. They always give me unconditional support and encouragement. I would like to thank my brother, Sang-uk, and my maternal grandparents. Without them, I would probably not have been at this point in my life. Especially, I would like to express my best gratitude to my wife, Hyojin as my lifetime companion who has profoundly influenced the way I view everything. She has been understanding me with sincerity. No word can express the love and gratitude that I feel for these six people. I sincerely would like to dedicate my dissertation to my family.

TABLE OF CONTENTS

DEDICATION	i
ACKNOWLEDGEMENTS	ii
TABLE OF CONTENTS	iii
LIST OF FIGURES	v
NOMENCLATURE	ix
Chapter 1. Introduction	1
1.1 Semiconductor Nanowires	1
1.2 Scope of Dissertation	1
Chapter 2. Laser-Assisted Direct Growth of Silicon Nanowires in a Localized Area via Thermal Activation	3
2.1 Overview	3
2.2 Experimental Setup	4
2.3 Thermal analysis & determination of temperature	5
2.3.1 Heating via laser absorption by thin film	5
2.3.2 Heating via laser absorption by catalytic Au nanoparticles	7
2.3.3 Determination of laser-induced temperature increase	8
2.4 Experimental Results and Discussion	9
2.5 Summary	14
FIGURES	
Chapter 3. Detail Investigations on the Mechanism of Laser-Assisted Fast Growth of Silicon Nanowires	23
3.1 Overview	23
3.2 Experimental Setup	24
3.3 Experimental Results and Discussion	25
3.3.1 Fast nucleation of laser-assisted growth of silicon nanowires	26
3.3.2 Catalyst size- and temperature-dependence of nucleation time	27
3.3.3 Catalyst size-dependence of activation energy	28
3.3.4 Branched growth of silicon nanowires	29
3.4 Summary	30
FIGURES	

Chapter 4. Laser Induced Nanoscale-Selective Direct Growth on Demand by Optical Near-Field Technique	39
4.1 Overview	39
4.2 Experimental Setup	40
4.3 Theoretical Basis	41
4.3.1 Local temperature of a gold nanoparticle by surface plasmon	41
4.3.2 Direct laser absorption on grown silicon nanowires	42
4.4 Experimental Results and Discussion	43
4.5 Summary	47
FIGURES	
Chapter 5. Electrically Biased Tip-Assisted Growth of a Single Silicon Nanowire	54
5.1 Overview	54
5.2 Experimental Setup	55
5.3 Experimental Results and Discussion	56
5.3.1 Selective and controlled growth of a single SiNW by an e-biased sharp tip	56
5.3.2 Electrostatic force for pulling a SiNW from a gold catalyst	57
5.4 Summary and Further study	58
FIGURES	
Chapter 6. Conclusions and Future directions	66
6.1 Summary	66
6.2 Future directions	67
APPENDIX	69
REFERENCES	71

LIST OF FIGURES

Figure 2-1.	Schematic diagram of laser-assisted Si nanowire growth setup.....16
Figure 2-2.	Results of thermal analysis describing laser-induced heating of 2 μm thick silicon film on fused silica wafer. Substrate side illumination and film side illumination cases are compared in each plot. (a) Calculated temperature at the reaction center (center of laser beam on film top) as function of illumination laser power, (b) temperature profile along depth direction at laser beam center, z, and (c) temperature profile along radial direction on film top, r. In (b) and (c), laser powers of ~ 36.9 mW and ~ 38.6 mW were used for substrate side and film side illumination cases, respectively to reach $\sim 500^\circ\text{C}$ at the reaction center.....17
Figure 2-3.	Scanning electron microscope (SEM) images of laser grown nanowires for comparison of the Si nanowires growth depending on laser illumination direction (a) film side illumination, (b) substrate side illumination. Laser power measured after focusing lens in the laser beam path. Zoomed-in image for ~ 44 mW laser power and 10 s illumination time case, (c) for film side and (d) substrate side illumination case.....18
Figure 2-4.	Scanning electron microscope (SEM) images of laser grown nanowires (substrate side illumination, laser power of ~ 59.3 mW and 5 s illumination time). Overall growth regimes are seen within a single growth spot due to temperature profile induced by gaussian laser beam profile. Marked regions from (1) to (4), corresponding to the maximum to the minimum local temperatures. Overall growth regimes are shown in (a), and further zoom-in images for the reasonable growth regimes in (b).....19
Figure 2-5.	Scanning electron microscope (SEM) images of laser grown Si nanowires upon film side laser illumination by various laser power levels and illumination time. The scale bars in the figures are 1 μm20
Figure 2-6.	Scanning electron microscope (SEM) images of laser-grown Si nanowires upon substrate side laser illumination by various laser power levels and illumination times. The scale bars in the figures are 1 μm21
Figure 2-7.	Kinetics of laser-assisted nanowire growth for the substrate side laser illumination case. (a) Plot of length of nanowires with respect to growth time and illumination laser power level. Illumination laser power and experimentally estimated temperature are marked in the figures. (b) Plot of Growth rate (R_{growth}) with respect to inverse of laser power ($1/P$). Growth rate was measured from linear curve section (early growth stage) of (a)..22
Figure 3-1.	A schematic diagram for laser induced local SiNWs growth system.....31

Figure 3-2.	Scanning electron microscope image of SiNWs grown on a 4.5 μm amorphous silicon film with 50 nm AuNPs by focused laser of which illumination time was varied from 1-30 s and power from 20-45 mW. The scale bar in the figure is 20 μm	32
Figure 3-3.	The length of SiNWs as a function of growth time at laser power from 20 mW to 40 mW which was measured from Figure 3.2.....	33
Figure 3-4.	Scanning electron microscopes images representing the stages just prior to nucleation, 8 ms (a), just after nucleation, 10 ms (b), 20 ms (c), and 100 ms (d) for 50 nm colloidal Au nanoparticles. Laser power was fixed at 45 mW and P_{SiH_4} was maintained at 6.5 Torr with flow rate of 200 sccm.....	34
Figure 3-5.	Nucleation time measured for laser power from 25 mW to 45 mW, corresponding the temperature.....	35
Figure 3-6.	The nucleation time with respect to different catalyst sizes (50 nm (blue) and 100 nm (red)) at varied laser power from 25 mW to 45 mW representing the temperature. The nucleation time is a function of the inverse of temperature in a semi-logarithmic scale.....	36
Figure 3-7.	Scanning electron microscope (SEM) images of laser-assisted growth of SiNWs with various time at fixed laser power of 25 mW. Au catalysts are 100 nm in diameter. (a) and (b) are for 20 s and 30 s, respectively. The scale bars in the figures are 1 μm	37
Figure 3-8.	Scanning electron microscope (SEM) images representing early stage of growth of SiNWs from 140 nm diameter AuNPs for 1 s (a) and 2 s (b) respectively. Laser power was fixed at 25 mW Scale bar in the figures is 200 nm.....	38
Figure 4-1.	A schematic diagram for optical near-field thermal triggered nanowire growth system.....	48
Figure 4-2.	Scanning electron microscope (SEM) image of SiNWs grown by indirect (a) and direct (b) heating of catalysts under far field focused laser beam. The scale bars in the figures are 1 μm	49
Figure 4-3.	Scanning electron microscope (SEM) image of SiNWs grown by minimal direct heating of catalysts under far-field focused film-side laser illumination with assistance of substrate-side laser illumination (72 mW). Film-side laser is illuminated at power of 2 mW for 30 s (a), 3 mW for 20 s (b), and 3 mW for 30 s (c), respectively. The scale bars in the figures are 1 μm	50
Figure 4-4.	Scanning electron microscope (SEM) image of SiNWs grown by minimal direct heating of catalysts under near-field focused film-side laser illumination with assistance of substrate-side laser illumination (72 mW). Film-side laser is illuminated at power of 3 mW for 30 s (a) and 4	

	mW for 20 s (b), respectively. The scale bars in the figures are 1 μm	51
Figure 4-5.	Calculated lateral temperature profiles at top surface of a-Si film in the center of the laser spot with different film-side laser illumination beam size coupled with supportive substrate-side laser local heating for local heating of the top surface by 400 °C	52
Figure 4-6.	Calculated lateral temperature profiles at top surface of a-Si film in the center of the laser spot with different film-side laser illumination beam size coupled with supportive local substrate heating by substrate-side focused laser illumination and with global substrate heating by substrate heater (350 °C) for heating by 400 °C	53
Figure 5-1.	A schematic diagram (a) for controlled growth of SiNW by an electrical biased sharp tip (b) which typically has 10 nm in radius of the tip. The Tip was ESP (0.01-0.025 $\Omega\text{-cm}$, Veeco Instruments Inc.) The scale bar in (b) is 10 μm	60
Figure 5-2.	A single SiNW among AuNPs randomly distributed on the amorphous silicon substrate AuNPs was directed at 55° by employing DC biased sharp tip of which total voltage was 46 V. Positive and negative biases were applied to the sharp tip and the sample, respectively. A focused laser illuminated in the interface between a-Si film and fused silica substrate heated up the catalysts within heat affected zone to activate the growth of SiNWs. (a), (b), and (c) respectively show an as-grown nanowire at rotation angle of 0, 90 and 180° with tilted angle of 35°. The bias voltage was 46 V. Laser was illuminated at 69 mW for 10 s. The scale bars in the figures are 200 nm.....	61
Figure 5-3.	SiNWs grown on the amorphous silicon film without an external bias. Laser was illuminated at 69 mW for 10 s. The scale bar in the figure is 500 nm.....	62
Figure 5-4.	SiNWs((b) for top view and (c) for 45° tilted view) grown by the DC positive biased plateau tip (a) which has 1.8 μm in diameter. The tip was PL2-CONTR (NANOSENSORS™). The bias voltage was 46 V. Laser was illuminated at 72 mW for 10 s. The scale bars in the figures is 1 μm	63
Figure 5-5.	Measured deflection of a sharp tip and a plateau tip at varied bias voltages. The sharp tip and the plateau tip was PPP-CONTR ($k = 0.2$ N/m, $R_{tip} = 10$ nm) and PL2-CONTR ($k = 0.2$ N/m, $R_{tip} = 1.8$ μm) from NANOSENSORS™, respectively.....	64
Figure 5-6.	Projected area of the catalyst onto the tip depending on its geometry. The field effective area ($2 \times \pi \times (10\text{nm})^2$) of the sharp tip (a) is smaller than	

that of projected area ($\pi \times (20 \text{ nm})^2$) of the catalyst. On the other hand, the surface of the plateau tip ($\pi \times (0.9 \mu\text{m})^2$) is much larger than the size of the catalyst, respectively.....65

NOMENCLATURE

- c_L = silicon content of the liquid phase
 c_S = silicon content of the solid phase
 d = catalyst diameter [nm]
 D_L = diffusion coefficients of silicon through liquid
 D_S = diffusion coefficients of silicon through solid gold
 h = convective heat transfer coefficient [$\text{W}/\text{m}^2\cdot\text{K}$]
 I_0 = incident laser intensity [W/m^2]
 k_e = coulomb force constant
 k_m = thermal conductivity of surrounding medium [$\text{W}/\text{m}\cdot\text{K}$]
 l_{opt} = optical penetration depth [nm]
 $N_{particle}$ = number of particles within laser spot
 P = laser power [W]
 P_m = threshold laser power [W]
 P_{SiH_4} = partial pressure of SiH_4 [Torr]
 Q_{abs} = absorption efficiency
 r_{laser} = laser focal spot radius [μm]
 $r_{particle}$ = particle radius [nm]
 R = reflectivity of laser from Si film
 t_{st} = steady time taken as a time to reach 1/e of maximum temperature increase [sec]
 T = temperature [K]
 z_f = Si film thickness [m]

Greek Letters

- α = the specific free energy of the catalyst surface
 α_{Si} = thermal diffusivity of silicon thin film [m^2/sec]
 ε_0 = electric constant [F/m]
 λ = wavelength of the laser beam [nm]
 Ω = the atomic volume of Si [m^3]

$\Delta\mu$ = the effective difference between the chemical potentials of Si in the vapor phase and in the catalyst

CHAPTER 1

INTRODUCTION

1.1 Semiconductor Nanowires

Semiconducting nanowires have been basic components in a wide range of future generation devices ranging from photonics^{1,2,3,4,5,6,7} and electronics^{8,9,10,11,12,13,14,15} to energy conversion and storage,^{16,17,18,19,20,21,22,23} biological sensing,^{24,25,26,27,28,29,30} and nano-electro-mechanical systems (NEMS)^{31,32} due to their unique properties^{16,17,18} stemming from the one-dimensional structure that is unseen in the bulk form. The Vapor-Liquid-Solid (VLS) growth mechanism has been a very promising fabrication method for semiconducting nanowires since 1960s' introduced by Wagner and Ellis³³ due to high aspect ratio achievable without conventional lithography processes. However, to realize the semiconducting nanowire-based device, new techniques must be developed that will enable precise layout and assembly of heterogeneous components into functional 'superblocks'. Even though high level of compositional and orientation control in nanowire growth has been achieved, the post-synthesis assembly steps even by state-of-the-art optical or optoelectronic tweezing^{34,35} are not yet sufficient for allowing high spatial and angular precision. As an efficient route towards this goal, several research groups have demonstrated direct growth of nanowires^{36,37} or nanotubes^{38,39,40,41,42} on specific parts of the sample platform by local laser illumination. However, understanding of the laser-assisted nanowire growth is still in infancy. Especially, laser-assisted growth of semiconductor nanowires under reasonable control has not yet been reported, preventing the laser-assisted growth technique from being actively used in a variety of application fields. In this thesis, laser-assisted growth of SiNWs is in detail studied. Recent results on highly selective and controlled direct growth of a single SiNW will be presented.

1.2 Scope of Dissertation

In chapter 2, laser-assisted silicon nanowire (SiNW) growth based on vapor-liquid-solid (VLS) mechanism is studied. By spatially confining the nanowire growth

region via focused laser beam illumination, multi-parametric study is carried out in a single platform by controlling the process conditions such as growth time, laser power, and laser illumination direction.

In chapter 3, with arbitrary temporal resolution by taking advantage of the fast localized heating capability of laser that cannot be achieved in conventional furnace conditions, a detailed investigation is carried out on the mechanism of laser-assisted growth of SiNWs. Specifically, catalyst diameter and temperature dependence of nucleation time and catalyst diameter dependence of activation energy required for the diffusion of silicon through solid Au are experimentally investigated.

Chapter 4 presents selective growth of a single silicon nanowire (SiNW) by employing an optical near-field technique. A nanoscale heat source is achieved by a focused laser coupled with an optical near-field probe. Due to limited thermal budget obtained from the probe, focused laser illumination is spatially overlapped. Therefore, the function of optical near-field based illumination is to trigger the process with high spatial resolution. By combining the two illumination schemes, optimal conditions for highly selective growth of SiNW are explored with relevant heat transfer analysis.

In Chapter 5, further effort to improve the orientation of SiNW growth is made by implementing electrically biased tip. Amorphous silicon film is selected to facilitate the arbitrary crystalline direction from the substrate. The plasma ignition is suppressed through the current limit. The electrostatic force is examined as dominating driving force for direction control. As a calibration step, the deflection of the tip with respect to applied bias voltage is measured.

Chapter 6 summarizes and highlights the conclusion of the present work and suggests possible future research directions.

CHAPTER 2

LASER ASSISTED DIRECT GROWTH OF SILICON NANOWIRES IN A LOCALIZED AREA VIA THERMAL ACTIVATION

Nanoscale-synthesized materials hold great promise for the realization of future generation devices. In order to realize this exceptional promise, new techniques must be developed that will enable the precise layout and assembly of the heterogeneous components into functional ‘superblocks’. Direct synthesis of nanostructures via laser-assisted chemical vapor deposition process is one promising route. In Chapter 2, laser-assisted silicon nanowires growth based on vapor-liquid-solid (VLS) mechanism are studied. By spatially confining the nanowire growth region via focused laser beam illumination, a convenient way to examine multiple growth parameters (temperature, time, illumination direction) is developed, thereby elucidating fundamental mechanisms of laser-assisted growth in a single sample configuration. Furthermore, a superior capability of direct synthesis of multi-parametric nanostructures is demonstrated for the purpose of practical rapid patterning.

2.1 Overview

Nanoscale-synthesized materials hold great promise for the realization of future generation devices spanning diverse fields including nanowire-based applications in fields such as energy conversion^{21,19} and energy storage,^{23,43} optoelectronics,^{44,45} and biotechnology.^{46,47} To realize this promise, new techniques must be developed that will enable the precise layout and assembly of heterogeneous components into functional ‘superblocks’. Even though high level of compositional and orientation control in nanowire growth has been achieved, the post-synthesis assembly steps even by state-of-the-art optical or optoelectronic tweezing^{34,35} are not yet sufficient for allowing high spatial and angular precision. As an efficient route towards this goal, several research groups have demonstrated direct growth of nanowires^{36,37} or nanotubes^{38,39,40,41,42} on specific parts of the sample platform by local laser illumination. Although additional catalyst related mechanisms such as vapor-liquid-solid (VLS) maybe involved, the

laser-assisted nanowire (nanotube) growth essentially falls into the category of laser chemical vapor deposition (LCVD) that has been actively explored for a few decades¹⁸ as an extremely versatile materials synthesis technique enabling the formation of technologically attractive microstructures of well-defined dimensions in a single-step maskless process.⁴⁹ The decomposition of precursor molecules in LCVD can be activated either thermally (pyrolytic process) or non-thermally via sufficient photon energy typically from ultraviolet laser radiation (photolytic process) or by a combination of both (photophysical process). The pyrolytic LCVD offers major advantages of high-purity at fast deposition rates and hence has been preferred in achieving high quality epitaxial nanowire growth in conjunction with VLS mechanism. While fundamental mechanisms in traditional LCVD have been studied in great detail^{49,50} understanding of the laser-assisted nanowire growth is still in its infancy. Especially, laser-assisted growth of semiconductor nanowires under reasonable control has not yet been reported, preventing the laser-assisted growth technique from being actively used in a variety of application fields.

In this chapter, laser-assisted silicon nanowire growth is presented. A focused laser beam (continuous wave laser of green wavelength) was illuminated onto Au nanoparticles of ~30 nm diameter assembled on thin amorphous silicon film (~2 μm) deposited on fused silica wafer. Various growth conditions (temperature, time, and laser illumination direction) are examined for a single sample domain in order to elucidate fundamental laser-assisted growth mechanisms, taking advantage of lasers in terms of precise control of local growth temperature and growth time. The effect of laser illumination direction (film side and substrate side illumination) on the silicon nanowire growth is explored in conjunction with local field enhancement of laser beam in the nanostructures. It is noted that the overarching aim of this experiment is to demonstrate the promise of direct and localized growth of nanostructures by lasers.

2.2 Experimental Setup

Figure 2-1 shows a schematic diagram of laser-induced nanowire growth system. The sample configuration tested in this experiment was Au nanoparticles of 30 nm diameter (Tedpella Inc.) assembled on amorphous silicon film of ~2 μm thickness sputtered on fused silica wafer (Hoya) in room temperature. Continuous wave (CW) laser beam of 514.5 nm wavelength (Ar ion laser, Innova, Coherent) was focused via an objective lens on the Si film both through the transparent substrate and against the film side at ~10 μm focal spot diameter. The ~2 μm film thickness was selected since this thickness exceeds the optical penetration depth of laser into the silicon film (measured value by an ellipsometer was ~0.171 μm) in order to minimize direct Au catalyst heating effect in case of substrate side illumination but at the same time

guarantee sufficient absorption of energy from laser by the film for both illumination cases. Processing gas was ~0.9% SiH₄ diluted in Helium. For gas environment control, the sample was enclosed within a custom-made vacuum chamber, equipped with optical windows allowing optical access via a dual upright/inverted microscope scheme. The chamber is first evacuated (~1 mTorr) followed by Ar gas flowing at ~200 sccm for 10 minutes for purging purpose. Then, processing gas was introduced at ~200 sccm by a mass flow controller, maintaining target total chamber pressure at ~650 Torr (set at relatively high pressure due to limited SiH₄ gas concentration)⁵¹ by an exhaust valve controller. Laser power (i.e. growth temperature) control was achieved by an attenuator set (a half-wave plate and a polarizing beam splitter), and laser illumination time (i.e. growth time) was precisely controlled by an optical switch in the range of ~1-60 s. As will be separately discussed in the later section, short heating and cooling time scale by laser (typically < ~10-100 μs for continuous wave laser upon micron scale focusing)⁵⁰ enables extremely precise control of growth time compared to the conventional furnace heating (> ~10 s time control accuracy).⁵¹ Multiple reaction temperature conditions can be easily plugged in a single sample once steady gas condition is achieved (typically in a few minutes), and multiple gas conditions can be also tested since no growth occurs as long as laser is off during the gas stabilizing process. Both transmission and reflection optical microscope images are utilized for *in-situ* monitoring of the laser-assisted growth, detecting the evolving CVD process. Ex-situ characterization was also performed by a scanning electron microscopy (dual beam SEM/FIB system, FEI).

2.3 Thermal Analysis & Determination of Temperature

As the first step to elucidate the laser-induced growth mechanism, it is crucial to understand laser-induced temperature temporal evolution and spatial profile across the reaction spot. Absorption of laser power by thin Si film and Au particle determines the induced heat source term. For the substrate side illumination, the film heating plays a major role in the growth, especially when film thickness is much larger than the optical penetration depth of laser as in the current configuration. On the other hand, the extra heating via direct absorption of laser energy by Au nanoparticles becomes important for the film side illumination or when film thickness is small (< optical penetration depth), as will be also considered.

2.3.1 Heating via laser absorption by thin film

Source term inside the film is in the form of volumetric heat source defined by reflectivity from the film (estimated using refractive indices measured by an ellipsometer, ~ 0.38 and ~ 0.23 for film side and substrate side illumination, respectively), the optical penetration depth through the Si film (measured value of ~ 170 nm), and Gaussian profile of laser at its focus (~ 10 μm diameter; $1/e^2$ definition, measured by knife edge method). Considering the low heat transfer losses from the sample surface, a steady temperature profile is essentially determined when the laser-induced source term is balanced by the diffusive loss. The time to reach steady temperature (t_{st}) roughly scales as $\sim r_{\text{laser}}^2 / \alpha_{\text{Si}}$ for silicon film, reasonably neglecting the convective and radiative losses (r_{laser} is laser focal spot radius and it is also an effective heat penetration depth at steady state,⁵⁰ and α_{Si} is thermal diffusivity of silicon thin film), and becomes $\sim O(10$ $\mu\text{s})$.

For further understanding of the laser-induced heating characteristics, three-dimensional heat equation was numerically solved for both film and substrate considering the volumetric heat source term in the film and radiative/convective losses to the surrounding medium (losses almost negligible).⁵² Figure 2-2 shows representative plots of calculated temperature profiles. According to temperature evolution on top of Si film and center location of laser beam, i.e. reaction center (not shown here), t_{st} (taken as a time to reach $1/e$ of maximum temperature increase) was ~ 10 μs upon film side illumination as expected above. However, t_{st} at the reaction center upon substrate side illumination is extended (~ 15 μs) due to longer thermal diffusion path from source location (\sim bottom of the film) to the reaction center. In Figure 2-2(a), steady state temperature (taken values after sufficiently long time elapse; 400 μs) at the reaction center is plotted as function of illuminated laser power. The linear dependence between laser power and the reaction center temperature is utilized for the experimental determination of laser-induced temperature increase, as will be explained in later section. Temperature profiles along film thickness direction (through the center axis) and lateral (radial) direction on Si film surface are displayed in Figure 2-2(b) and 2-2(c), respectively, for the laser powers leading to temperature of $\sim 500^\circ\text{C}$ at the reaction center (36.9 mW for substrate side illumination and 38.6 mW for film side illumination). While the location of peak temperature in the thickness direction is at the top of the film for film side illumination, for substrate side illumination it is on the film-substrate interface, as shown in Figure 2-2(b). The fact that higher laser power requirement is needed for in the case of the film side illumination to reach similar temperature at the reaction center is attributed to the lower reflectivity in conjunction with heat transport from heat source location. The lower reflectivity for the substrate side illumination (i.e. absorption of more laser energy into the film) essentially leads to higher peak temperature for film-substrate interface. However, steady temperature on top of the film

is lower than that at the film/substrate interface due to heat diffusion across the film. At the specific case of $\sim 10 \mu\text{m}$ laser beam diameter, the temperature at the reaction center induced by substrate side illumination is lower than that by film side illumination at heat balance. A similar trend has been observed in larger laser spots.⁵³ However, for smaller laser spots that are of interest in order to achieve higher spatial resolution nanowire patterning, this trend can be reversed; for example, calculations for $\sim 5 \mu\text{m}$ laser spot diameter show that the temperature at the reaction center by substrate side illumination is lower than that by film side illumination due to increased three-dimensional thermal diffusion effect from smaller heat source.⁵² Temperature completely decays within $\sim 30 \mu\text{m}$ depth from top of the glass substrate, maintaining most of the substrate thickness under room temperature (Figure 2-2(b)), and demonstrating depth-wise localized heating capability of lasers. The lateral temperature profiles (Figure 2-2(C)) are close to the Gaussian laser beam profile with broadening by effective lateral diffusion lengths roughly matched to r_{laser} or $(\alpha_{\text{Si}} t_{\text{st}})^{1/2}$ as explained before. Similar diffusion length scaling is applied for depth direction (z) as well (Figure 2-2(b)). One can expect that in general thinner film would be more advantageous for achieving tighter lateral confinement of growth region for the substrate illumination case as long as the film thickness is sufficiently larger than the optical penetration depth. Based on the lateral temperature profile at steady state (Figure 2-2(c)), it is expected that precise adjustment of illumination laser power will allow lateral dimension of growth region smaller than actual laser beam spot size even with continuous wave laser heating.

2.3.2 Heating via laser absorption by catalytic Au nanoparticles

Effects of direct laser absorption by the metal particle catalysts are considered in respect to two different aspects; contribution to the overall temperature increase at the reaction spot (film), and localized heating of the catalytic particles themselves. For an approximate estimation of the overall temperature increase in the film via laser absorption in particles, simple calculations by Mie theory are performed assuming independent scattering regime (average number density of ~ 200 particles per $\sim (5 \mu\text{m})^2$ laser spot area, and corresponding average spacing between particles of $\sim 360 \text{ nm}$).⁵⁴ For film side illumination, ratio of absorbed laser power by Au nanoparticles and Si thin film within laser spot is roughly scaled as $(r_{\text{particle}} / r_{\text{laser}})^2 Q_{\text{abs}} N_{\text{particle}} / (1 - R)$ (where r_{particle} is particle radius, Q_{abs} , absorption efficiency, N_{particle} , number of particles within laser spot, and R, reflectivity of laser from Si film), and becomes ~ 0.005 ($\sim 0.5 \%$) under current experiment conditions, showing that direct absorption by Au nanoparticles does not contribute to the overall temperature increase near the laser

spot. This ratio is even smaller for substrate side illumination since approximate incident laser intensity is attenuated by factor of $(1-R)\exp(-z_f/l_{opt})$ (where l_{opt} is optical penetration depth, and z_f , Si film thickness), further reducing the fraction of direct absorption by particles ($\sim 10^{-7}$). Direct laser heating of Au catalysts is less important when the substrate is well absorbing with respect to the laser wavelength unless number density of the catalysts is very large. On the contrary, if substrate is transparent for the laser illumination, direct laser heating of the catalysts is mainly responsible for the pyrolytically driven CVD process.

Even though the contribution of absorption in Au nanoparticles to the overall heating is negligible, local temperature of Au catalytic particles is still important since it governs the growth of nanowires in the case of film side illumination. Laser-induced temperature increase in the particles at steady state is calculated by balancing source (absorption) and loss to the surrounding medium. Major loss is through convection (conduction through the surrounding medium), safely neglecting radiative loss and conductive loss through the substrate due to high contact resistance.⁵⁵ Through the balance of $h(4\pi r_{particle}^2)\Delta T = I_0 Q_{abs}(\pi r_{particle}^2)$ and the approximation of $h \sim k_m / r_{particle}$ (I_0 is incident laser intensity, h , convective heat transfer coefficient, and k_m , thermal conductivity of surrounding medium), the temperature increase ΔT is estimated as $r_{particle} I_0 Q_{abs} / 4k_m$. As for film side illumination laser power of ~ 38.6 mW (leading to the reaction center temperature of $\sim 500^\circ\text{C}$), ΔT in Au nanoparticle is ~ 36 K for air medium and ~ 6 K for Helium environment. This temperature increase can be interpreted as an upper bound of heating in addition to the base heating from the silicon film, demonstrating the effect of plasmonic resonance^{36,37} in terms of resulting temperature increase. If the nanoparticles are on non-absorbing substrate, laser intensity higher by two orders of magnitude will be required for nanowire growth. However, it should be noted that in actual growth process local temperature and/or phase (molten) of Au catalysts will dynamically modify the absorption characteristics and additional absorption onto the pre-grown part of Si nanowires will lead to secondary heating of pre-grown structures,⁵⁶ for the film side illumination case.

2.3.3 Determination of laser-induced temperature increase

Determination of laser-induced temperature is a necessary step for fundamental level studies on laser-based growth kinetics in actual experiments. Laser induced temperature increase in thin Si film on glass substrate has been measured by several techniques such as infrared emission measurement (pyrometry)⁴⁸ and reflectivity measurement including over the melting regime.⁵⁷ In this study, we

followed experimental procedure used by ref.⁵³P; essentially measuring melting threshold laser power and estimating temperature at lower laser power levels by assuming linear dependence of the temperature on the laser power (absolute temperature calibration enabled by melting temperature of $\sim 1410^\circ\text{C}$) as the linear dependence displayed in Figure 2-2(a) has been shown valid in a number of similar Laser-assisted Si CVD experiments.⁵³P Utilizing the experimentally measured melting threshold laser power (P_m) at similar gas environment (Helium environment, ~ 650 Torr and ~ 200 sccm) and Si film without Au catalysts, the temperature as function of laser power P was determined at $(1410-27)(P/P_m)+27$ ($^\circ\text{C}$), mainly for the purpose of assisting the kinetic analysis in the case of substrate side illumination.

2.4 Experimental Results & Discussion

Laser-assisted silicon nanowire growth

SEM images in Figure 2-3(a) and 2-3(b) show bird's eye views of laser-assisted Si nanowire growth results for film side illumination and substrate side illumination, respectively. It is highlighted that each spot displayed in the figures has experienced different growth parameters (laser power; growth temperature, and laser illumination time; growth time), allowing implementation of a wide parametric domain in a single sample configuration within tight spacing. This variation can be appreciated when compared to conventional furnace growth where altogether new sets of experiments would be required to span the same parametric space. Laser-assisted growth not only offers a convenient and systematic tool for exploring new types of growth mechanisms, but also, in practical aspect, the results show great promise on the direct growth of multi-parametric nanowires (e.g. length, composition) at a superior and arbitrary position accuracy in programmable manner. As discussed earlier, temperature profile is broadened from laser focal spot approximately by a factor of 2 (effective diffusion length of r_{laser} at steady state). However, broadened Gaussian-like temperature profile allows the growth spot size smaller than laser focal spot size (examples shown in Figures 3, 5 and 6) through precise control of laser power. The size of growth spot can be further reduced by use of tighter focus or optical near-field⁵⁸ and/or time modulation of laser illumination to reduce the effective thermal diffusion length. Reversely, the growth spot size can be readily expanded to the desired spatial extent, implying great flexibility in multiscale nanowire patterning by lasers.

The qualitative difference in growth trend depending on the laser illumination direction is clearly shown in Figure 2-3. For laser power in the range of ~ 23 -44 mW, film side illumination generated a dark region at the center of the growth spots. Zoom-in

images for ~ 44 mW laser power and 10 s illumination time case displayed in Figure 2-3(c) and its inset, illustrate that the central dark region was entirely covered with Si as a result of rapid Si CVD process. In this case, Si nanowires could be mainly observed at the spot periphery and over a noticeably large distance from the spot center. In contrast, reasonable nanowire growth trend was achieved upon substrate side illumination (Figure 2-3(d)); proper correlation of length with local temperature, still maintaining the diameter close to the Au catalyst size. Lateral extent of growth spot is essentially dictated by the temperature profile on the reaction spot.

Use of Gaussian laser beam profile allowed testing of broad range of laser power (temperature) dependence within a single laser spot. Zoom-in images in Figure 2-4 for substrate side illumination at the laser power of ~ 59.3 mW (5 s growth time) display different CVD regimes in a single laser-grown spot; as representative regimes indexed in the figure from the center of the laser spot to outer edge (decreasing local temperature), (1) covered with Si film of granular shape as result of rapid isotropic growth, (2) nanowire growth at significant simultaneous radial growth rate, (3) reasonable nanowire growth, and (4) nanowire growth at reduced growth rate. It is noted that laser-based nanowire growth allowed superior growth efficiency (i.e. number of grown nanowires per number of Au catalysts within laser illumination spot). Every Au catalyst reacted in accordance with local laser intensity (temperature) distribution. In comparison with furnace experiments using the same sample configuration (not shown here), the growth efficiency was significantly lower with frequent occurrence of non-reacting catalysts between grown nanowires. Higher growth efficiency by laser proves to be advantageous in terms of local growth temperature control capability.

The multi-parametric growth results shown in Figure 2-3 facilitate a systematic study on the laser-assisted growth mechanism. In addition to temperature control by adjusting laser power, accurate control of growth time by varying laser illumination time (1-60s) enabled comprehensive investigation on the transient behavior of the laser-assisted growth. In general, the respective parametric study revealed it was very difficult to achieve reasonable nanowire growth upon film side illumination. According to the transient behavior for film side laser illumination for various laser power levels (Figure 2-5), nanowires do grow in diameter close to the catalytic particle size at very early stage (e.g. 5 s by 19.6 mW laser power, and 1 s by 23.2 mW in Figure 2-5), but in subsequent growth process, frequently the nanowire diameter becomes significantly larger than the catalyst size. Intrinsic difference of heating by film side laser illumination from heating by substrate side illumination is in the enhanced absorption in local nanostructures of Au catalyst and pre-grown Si nanowire. This transient behavior supports the possibility that thickening of nanowires grown by film side illumination may be due to localized heating of grown nanowire (local absorption enhancement in the nanowires), leading to secondary Si CVD on the hot nanowire surface. Based on the reasonable growth inspected at early stage, the effect of enhanced catalyst heating seems to be still favorable. Another supporting evidence is that nanowires with diameter close

to the catalyst size are found near edge of illuminated region (i.e. the hot region not due to direct laser heating but because of laterally conducted heat from the hotter laser spot) as seen from most of the growth conditions. Upon laser power higher than ~ 29 mW, isotropic CVD prevails over the directional growth trend on the catalysts from very early stage (look the central region of 29.7 mW case in Figure 2-5) and direct Si CVD occurs even in the regions in-between the catalysts.

On the contrary, substrate side illumination (Figure 2-6) allowed wide range of processing window for reasonable nanowire growth (~ 25 -45 mW); nanowire grows lengthwise while maintaining diameter close to the catalyst size. In Figure 2-7(a), measured length of grown nanowires is plotted with respect to growth time, for different laser power levels. The length was measured from ~ 3 -10 nanowires near the center of the growth spot (i.e. peak temperature region) for the subsequent kinetic analysis purpose. The instantaneous growth rate was initially ~ 360 nm/s at the laser power level of ~ 44 -49 mW, and reduced at lower laser power levels. After almost a linear increase in length (i.e. constant growth rate) at the early stage of growth, the growth rate keeps decreasing possibly due to the decreasing catalyst temperature as the nanowire grows. The saturation trend in growth rate was observed even in furnace process,⁵¹ and was attributed to the decrease in catalyst temperature rather than the extended Si diffusion path since the catalyst remains located on top of nanowires throughout the VLS growth process. Under the current heating configuration (substrate side laser illumination), in a manner similar to substrate heater configuration, heat should be continuously conducted from the substrate to the catalyst through the growing nanowire stem. In an analogy to extended surface heat transfer (fin-like), finite heat loss through across the nanowire side-wall of nanowire (mediated mainly by collision of Helium molecules) will be responsible for the catalyst temperature reduction. When the laser power was ~ 30 mW or lower, initiation of the axial growth took longer than ~ 1 s (~ 60 nm length after 3 s at 30.4 mW, ~ 110 nm after 10 s at 27.9 mW, ~ 90 nm after 30 s at 25.3 mW, and ~ 50 nm after 60 s at 23.2 mW). In furnace growth under similar gas conditions,⁵¹ a finite time was needed to form precursor (i.e. nucleation time) as well; ~ 15 s at 400°C . In fact, experimentally determined temperature by 30.4 mW laser power was around 400°C . At that temperature, at which ~ 3 s was measured as a nucleation time, as the estimated temperatures are marked for all the cases of substrate side illumination in Figure 2-6 and 2-7. The discrepancy in the measured nucleation time comes from limited heating time control accuracy ($> \sim 10$ s) of the conventional furnace system used in ref,⁵¹ clearly proving highlighting an excellent heating time control and monitoring capabilities of lasers irradiations. On the other hand, at the laser power of 49.0 mW, nanowire became noticeably thick at the growth center after 10 s illumination (Figure 2-6), indicating rapid lateral growth at elevated temperature.⁵⁹ A similar situation occurred after 30 s at 44.1 mW laser power and after 60 s at 41.0 mW due to still high rate of lateral growth (not shown). Upon clear thickening, lengthwise growth rate significantly reduced, as

length and growth rate are plotted only for the timing before thickening in Figure 2-7(a). At further increased laser power (~ 54.2 mW) thin film is formed through isotropic growth on the catalysts and direct Si CVD process on bare Si surface, indicating the upper limit of Si nanowire growth. In general, nanowires grown at reduced laser power tends to be kinked, sticking onto and crawling on the substrate, as in a trend reported in furnace growth at temperature lower than $\sim 400^\circ\text{C}$.^{51,60} On the other hand, laser illumination for ~ 30 s or longer tends to generate complex nanowire growth behavior at relatively high laser power; thickened at laser power level of ~ 41 mW or higher, and joining neighboring nanowires at ~ 38 mW or higher (example shown in Figure 6, 41.0 mW and 30 s case). The joining of nanowires that occurred at elevated temperatures is attributed to random growth directionality promoted by the random crystalline direction in the tested amorphous silicon (a-Si) film, and the high number density of catalysts. As a result, optimal growth regime under current experimental configuration was formed at relatively short growth time range (< 30 s) and relatively high temperature (laser power). Assuming ideal directionality via use of single crystalline substrates, fundamental limit in maximum length is possibly governed by the heat loss through the side wall of grown nanowire as previously mentioned. At some point, and the reduced catalyst temperature upon due to fixed laser power and in conjunction with Au catalyst consumption will lead to self-termination of nanowire growth in conjunction with Au catalyst consumption. For the purpose of kinetic analysis, Figure 2-7(b) displays a logarithmic plot of measured nanowire growth rate (R_{growth}) with respect to the laser illumination power (P). The growth rate was measured from the linear part of the curves (early stage of growth) in Figure 2-7(a). The nice linear fitting between $\ln(R_{growth})$ and $1/P$ proves that 1) nanowire growth by substrate side laser illumination follows traditional Arrhenius behavior and 2) assumption of linear dependence between laser power (P) and local temperature in growth spot (T) was kinetically valid from the kinetics point of view. From the plot of growth rate with respect to the inverse of estimated temperature in Figure 2-7(c), the activation energy is calculated as ~ 66.8 kJ/mol, which is relatively smaller than a literature reported value by furnace process in similar condition (230 kJ/mol) for the catalyst particle size range of $\sim 3\text{-}40$ nm.⁵¹ Even though absolute comparison of relation between growth rate and temperature might not be easy due to actual difference in detailed configuration (e.g. catalyst configuration), it can be mentioned that one of the critical differences is in growth time resolution; ~ 15 s by furnace in their work. Keeping in mind reminding the growth rate variation in Figure 2-7(a) as well as the rapid decay in growth rate (within time scale $< \sim 10$ s) especially at relatively high growth temperatures ($> \sim 450^\circ\text{C}$), the growth rate estimated by averaging over time period longer than ~ 10 s is almost always lower than the peak growth rate averaged over shorter time. At medium growth temperature range ($400\text{-}430^\circ\text{C}$), the growth rate is relatively constant for longer time, alleviating the difference.

At the lower temperature ($< \sim 400^\circ\text{C}$), a finite nucleation time causes underestimation of the growth rate when the nucleation time is not negligible compared to the actual growth time. The current heating mechanism will effectively represent a similar substrate heater based growth configuration, albeit at superior time resolution. On the other hand, furnace heating might incur different actual temperature decay along the nanowire length due to the hot ambient gas. Nevertheless, limited time control resolution in most traditional growth methods either allows only average growth rate at reduced value or practically doesn't permit achievement of the maximum possible growth rate demonstrated by laser. In other words, use of laser enabled not only accurate monitoring of transient growth behavior, but also realized faster growth rate at shorter growth time (e.g. maximum growth rate of $\sim 360\text{ nm/s}$ was achieved by $\sim 3\text{ s}$ laser illumination at $\sim 569^\circ\text{C}$, while the reported maximum growth rate in furnace⁵¹ was $\sim 180\text{ nm/s}$ at relatively lower temperature of 495°C due to limited time resolution). Relatively lower activation energy in laser-assisted growth is partly explained by the difference in time resolution, but it should be also noted that localized CVD or growth by confined laser spot is advantageous in gas transport due to three-dimensional transport nature towards and from smaller reaction spot (CVD gas delivery, and exchange of reaction by-product such as Hydrogen) versus one-dimensional transport in wider reaction area cases.⁵⁰ More rigorous study is going on being conducted to unveil the limiting mechanisms (transport or reaction) in the laser growth by testing under different total and SiH_4 partial pressure conditions. However, it is postulated that the current growth process is governed by reaction limit, considering in view of the excessive impingement rate of SiH_4 molecules in current gas conditions ($\sim 1.5 \times 10^6$ per atomic site per second),⁵⁰ and also considering Si nanowire growth under VLS mechanism cannot be operated at very high temperature in contrast to the regular Si CVD. The importance of the measured peak growth rate at short time scale lies in that (1) it indicates an actual limit in typical VLS growth mechanism and its demonstration was possible via rapid heating control by laser, and (2) one can practically tune the process parameters to achieve maximum growth rate via laser-assisted method, supporting the promise of using this approach as a rapid and programmable processing tool.

Lastly, the laser illumination direction effect on the nanowire growth is briefly discussed. The nanowire growth threshold laser power by film side illumination was lower than that by substrate side illumination. As verified by both theoretical prediction (Figure 2-2(a)) and experimental temperature determination steps, the growth threshold in terms of temperature was also lower by film side illumination. This trend has been reported in the regular Si laser CVD studies as well for employing relatively large laser spots,⁵³ and where it was claimed that visible photon interactions with reactive species promote the reaction, initiating CVD process at reduced laser power or temperature when film side illumination is applied. In addition, film side illumination induces a

higher degree of excitation in Au catalysts, potentially assisted by plasmonic resonance. Such enhanced radiative energy coupling with the nanocatalyst may result in local temperature increase (explained in the previous section) and possibly excited electron mediated contribution to the reaction. However, dominant contribution of plasmonic resonance effect on the growth was limited only within very early stage of growth, rapidly followed by the secondary Si CVD on the surface of pre-grown nanowires thickening the nanowires. Further verification is underway by selection of different laser wavelengths. However, it should be noted that in the case of film side illumination constant laser power input does not necessarily correspond to constant catalyst temperature, which might not be a stable condition for the controlled epitaxial growth. Furthermore, highly dynamical change in laser absorption by the growing nanowire system depending on a number of factors such as local temperature, phase (e.g. molten, alloy), and shape of the Au catalysts as well as heat loss via the nanowire stem could cause unstable growth conditions.

On the contrary, in the case of substrate side laser illumination, the heating configuration is greatly simplified, essentially approaching substrate heater regime, when film thickness is sufficiently larger than optical penetration depth of the laser into the film material (optically thick film). Heating of Au catalysts also relies on the indirect heating from the film, hence guaranteeing a stable growth condition. Practical issues in adopting an optically thick regime: (i) the difficulty in laser alignment (invisible laser spot from film side), (ii) increase in required laser power, and (iii) lateral broadening of growth spot due to increased thermal diffusion. As for the former issue, *in-situ* monitoring of laser-driven growth spot itself and/or collinear coupling of longer wavelength probe beam should be effective solutions with respect to the alignment issues. As for the latter issue, a choice of shorter wavelength and/or use of more absorbing film material can mitigate the issues related to the laser power requirement as well as the spatial selectivity. In case of optically thin film (i.e. film thickness \ll optical penetration depth) as another extreme, laser induced catalyst heating configuration essentially approaches the film side illumination case. In contrast, in this case heat deposition on the substrate is significantly reduced and growth must mostly rely on direct catalyst heating.

2.5 Summary

In summary, laser-assisted silicon nanowire growth mechanism was experimentally explored using assembled Au nanoparticles on Si thin film and continuous illumination of green wavelength laser radiation either incident on the film surface or propagating through the transparent substrate. Film side illumination that is favorable for localized heating of catalytic nanoparticles through plasmonic resonance

allowed one-dimensional nanowire growth at very early stage. On the other hand, subsequent growth process was dominated by secondary Si deposition on the pre-grown nanowire. In contrast, substrate side laser illumination enabled indirect but stable heating of the catalytic nanoparticles through the locally hot substrate. Kinetic analysis confirmed that the growth follows the traditional growth trend. Laser-assisted thermally activated growth of silicon nanowires by introducing indirect heating of gold catalysts (substrate-side heating) will be studied in detail in Chapter 3. In addition, short growth time control by laser enabled the demonstration of nearly highest growth rate at given gas condition. Taking advantage of rapid and spatially confined heating capability of lasers, laser-assisted nanowire growth method is not only a convenient and systematic tool to explore new nanostructure growth mechanisms, but also a highly controllable mean to directly grow multiscale nanowires at an arbitrary position accuracy via accessing a wide space of processing parameters.

FIGURES

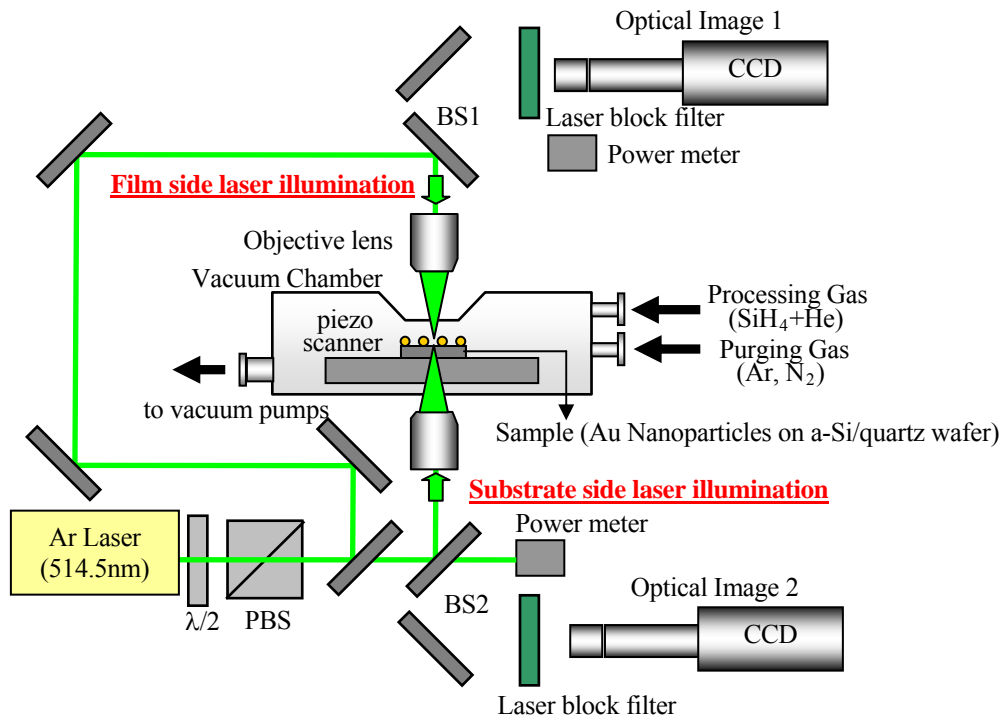


Figure 2-1. Schematic diagram of laser-assisted Si nanowire growth setup.

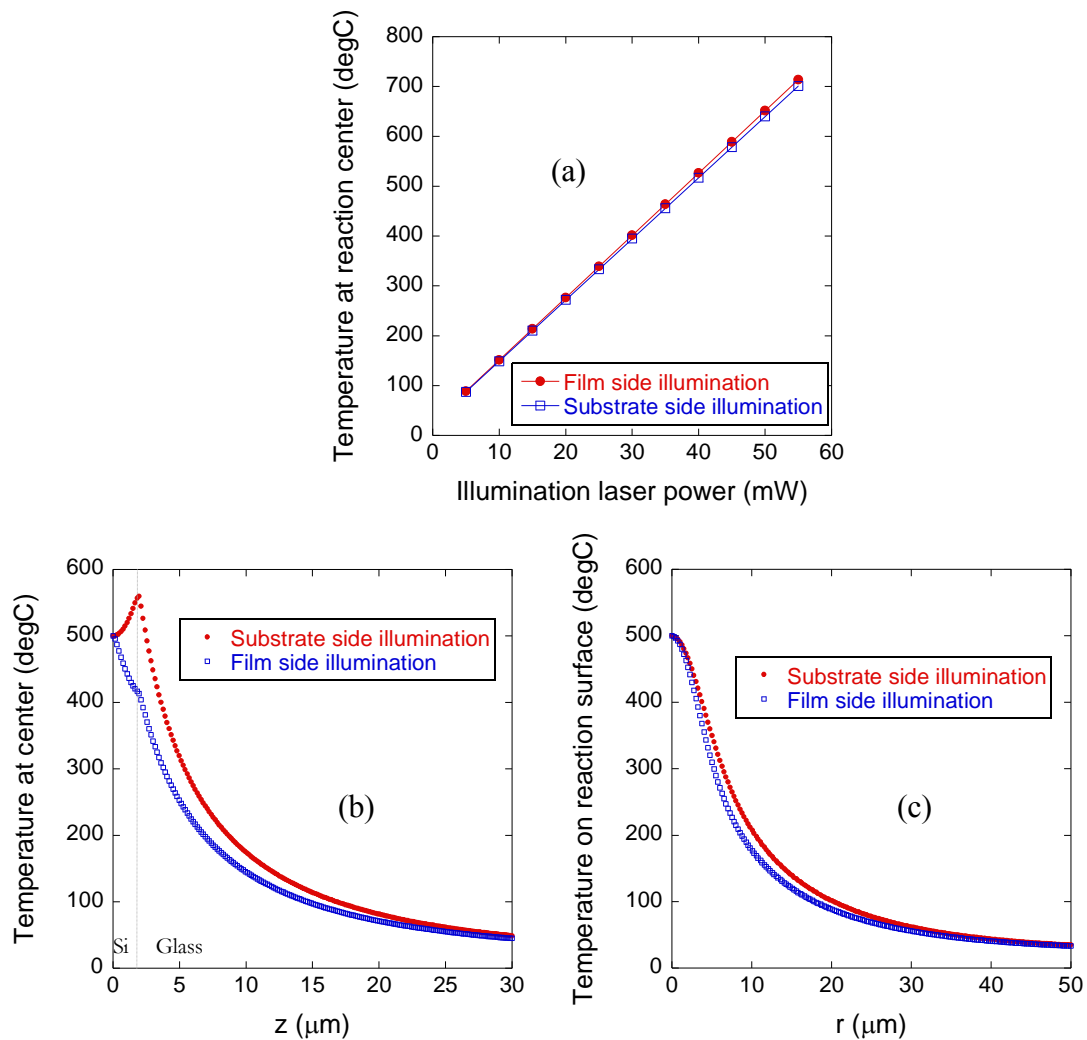


Figure 2-2. Results of thermal analysis describing laser-induced heating of 2 μm thick silicon film on fused silica wafer. Substrate side illumination and film side illumination cases are compared in each plot. (a) Calculated temperature at the reaction center (center of laser beam on film top) as function of illumination laser power, (b) temperature profile along depth direction at laser beam center, z , and (c) temperature profile along radial direction on film top, r . In (b) and (c), laser powers of ~ 36.9 mW and ~ 38.6 mW were used for substrate side and film side illumination cases, respectively to reach $\sim 500^\circ\text{C}$ at the reaction center.

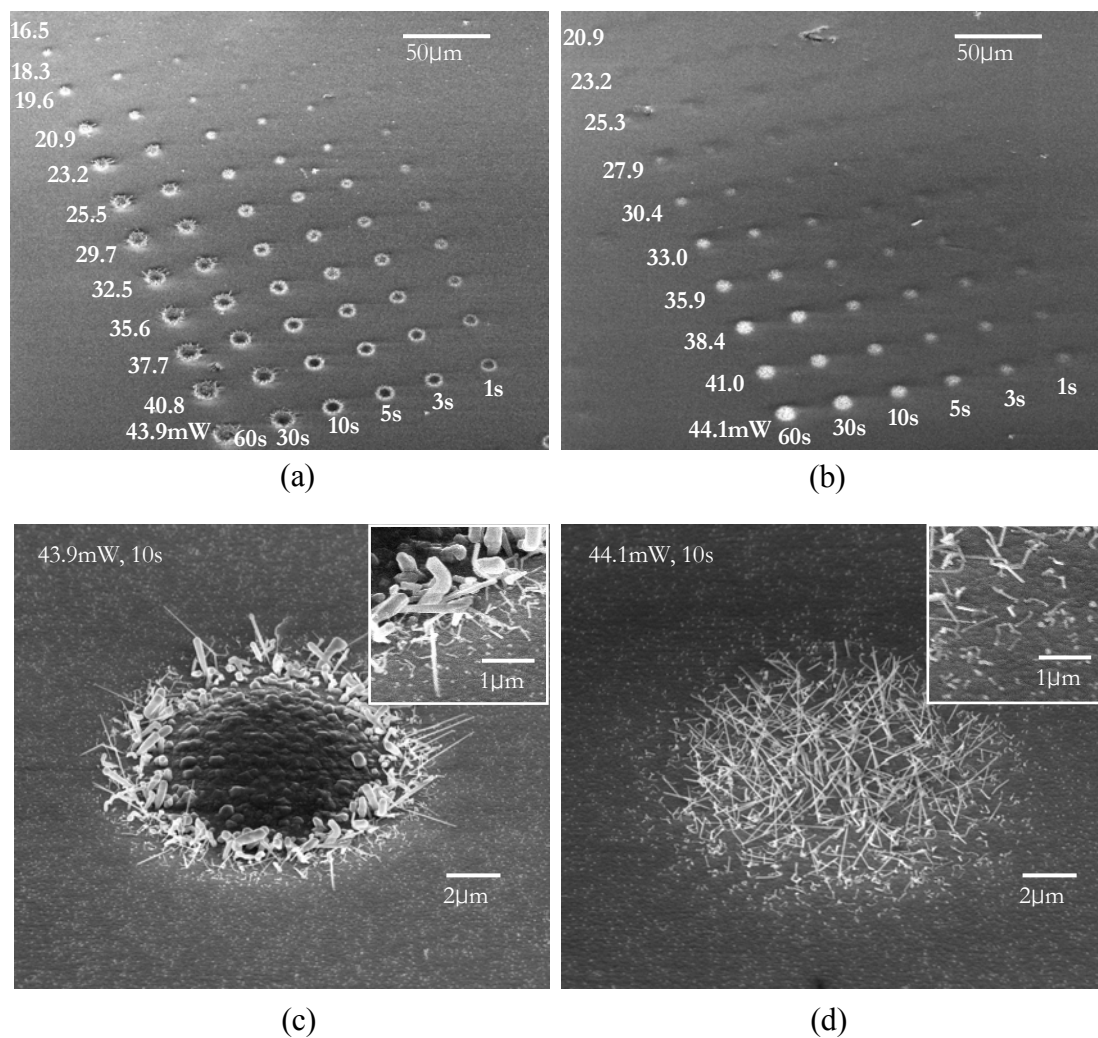


Figure 2-3. Scanning electron microscope (SEM) images of laser grown nanowires for comparison of the Si nanowires growth depending on laser illumination direction (a) film side illumination, (b) substrate side illumination. Laser power measured after focusing lens in the laser beam path. Zoomed-in image for ~44 mW laser power and 10 s illumination time case, (c) for film side and (d) substrate side illumination case.

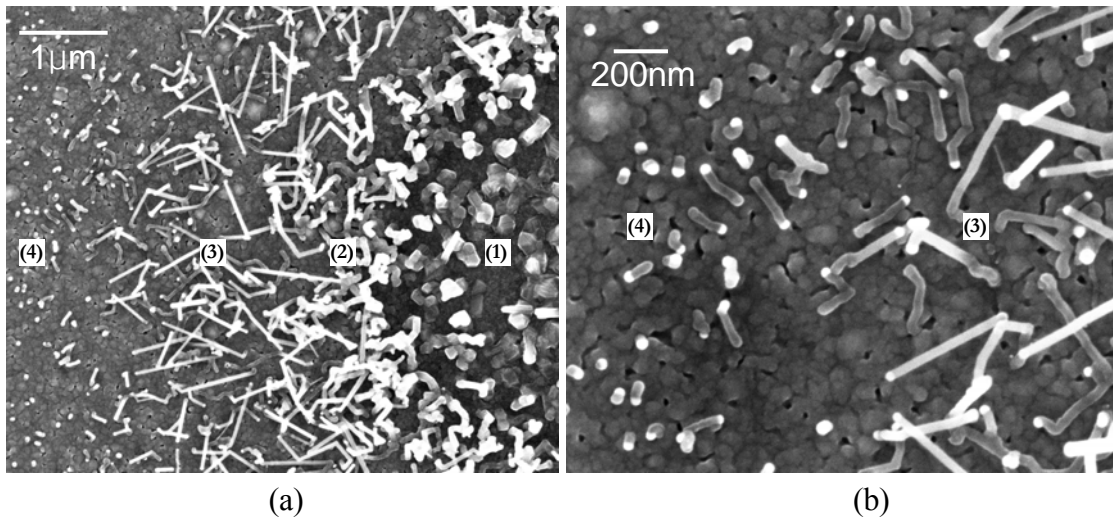


Figure 2-4. Scanning electron microscope (SEM) images of laser grown nanowires (substrate side illumination, laser power of ~ 59.3 mW and 5 s illumination time). Overall growth regimes are seen within a single growth spot due to temperature profile induced by gaussian laser beam profile. Marked regions from (1) to (4), corresponding to the maximum to the minimum local temperatures. Overall growth regimes are shown in (a), and further zoom-in images for the reasonable growth regimes in (b).

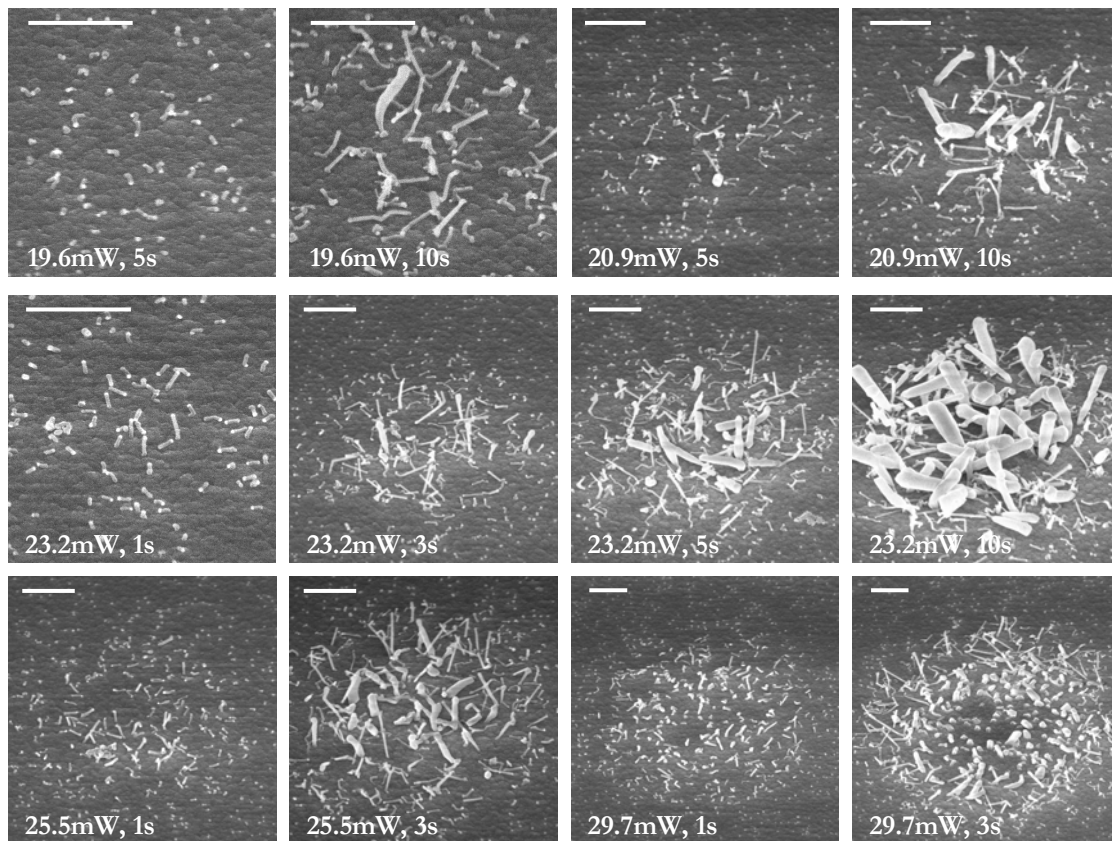


Figure 2-5. Scanning electron microscope (SEM) images of laser grown Si nanowires upon film side laser illumination by various laser power levels and illumination time. The scale bars in the figures are 1 μm .

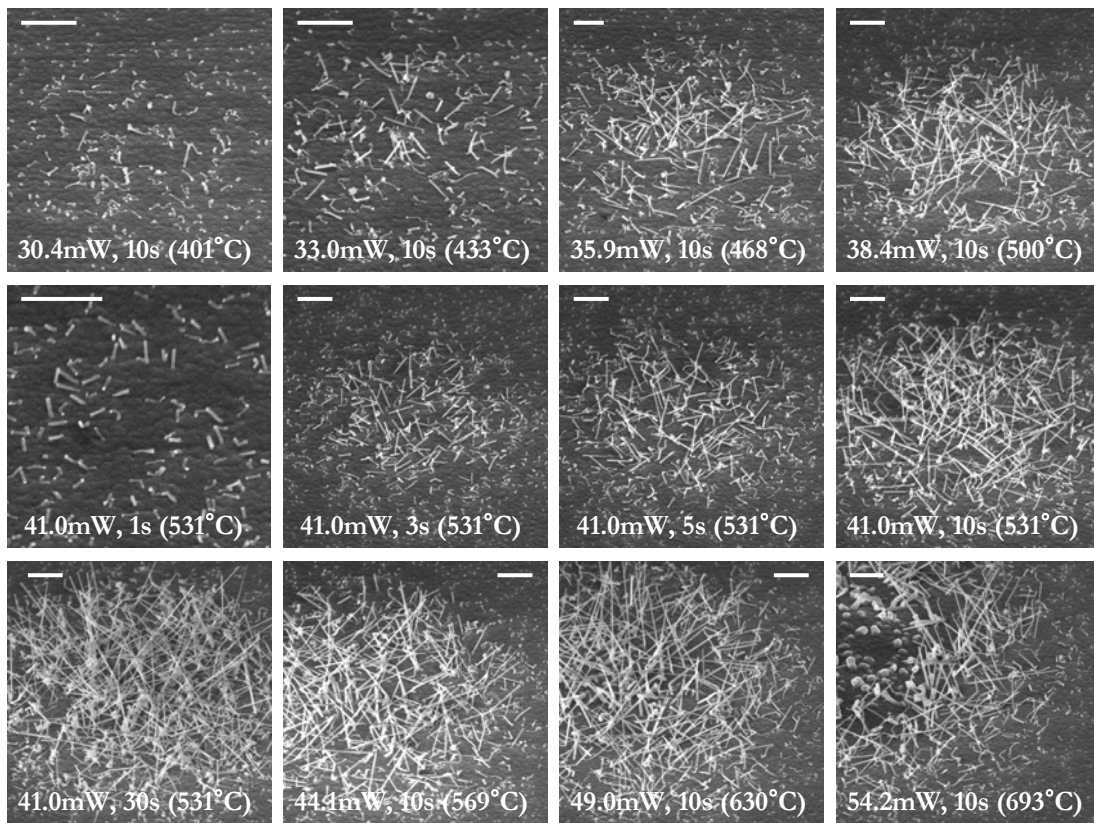


Figure 2-6. Scanning electron microscope (SEM) images of laser-grown Si nanowires upon substrate side laser illumination by various laser power levels and illumination times. The scale bars in the figures are 1 μm .

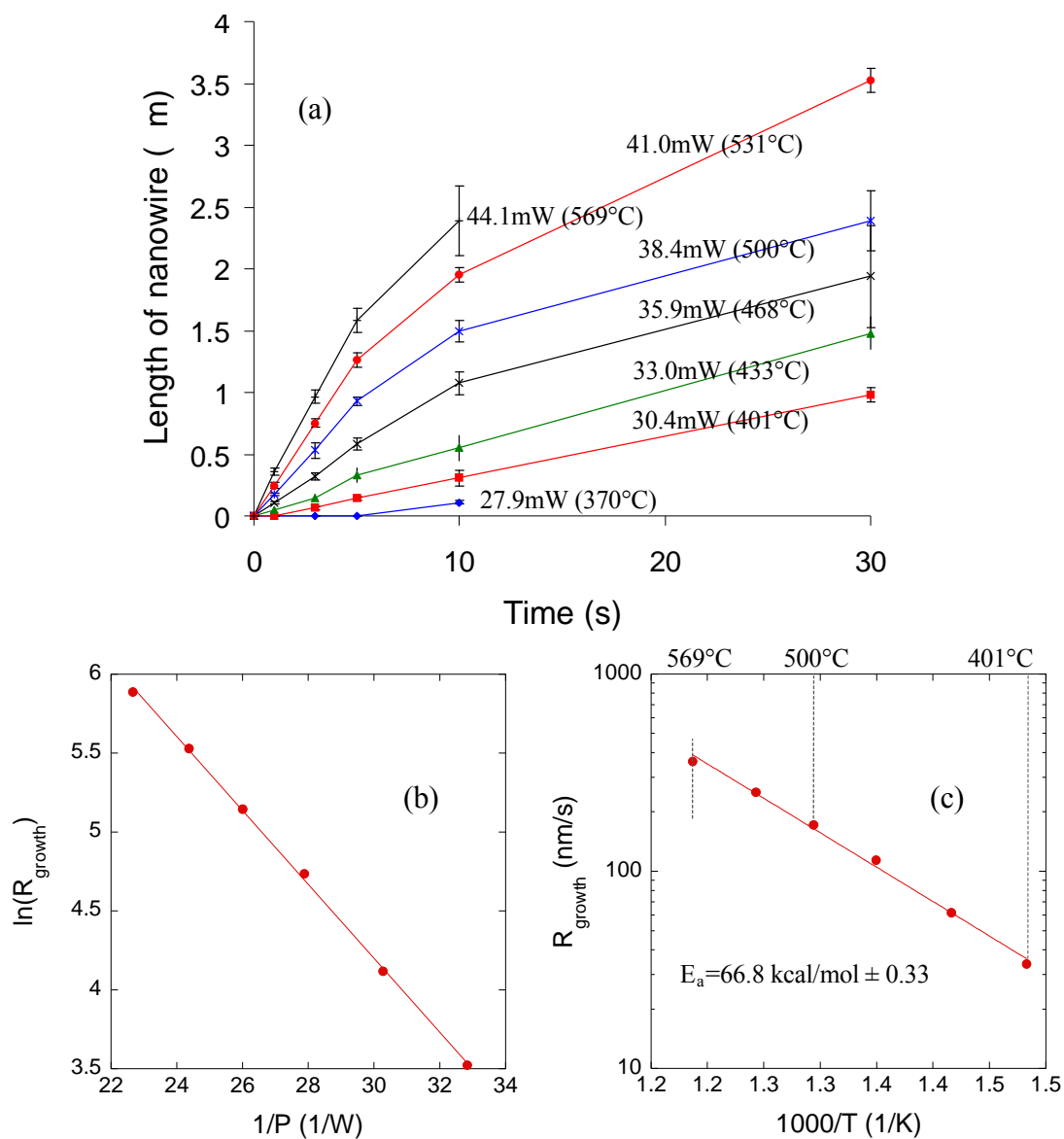


Figure 2-7. Kinetics of laser-assisted nanowire growth for the substrate side laser illumination case. (a) Plot of length of nanowires with respect to growth time and illumination laser power level. Illumination laser power and experimentally estimated temperature are marked in the figures. (b) Plot of Growth rate (R_{growth}) with respect to inverse of laser power ($1/P$). Growth rate was measured from linear curve section (early growth stage) of (a).

CHAPTER 3

DETAILED INVESTIGATIONS ON THE MECHANISM OF LASER-ASSISTED FAST GROWTH OF SILICON NANOWIRES

In Chapter 2, laser assisted direct growth of silicon nanowires (SiNWs) has been explored with respect to direct and indirect heating of the catalyst. It was shown that laser-assisted growth of SiNWs is thermally activated following Arrhenius like behavior as the catalysts are indirectly heated. This entails a useful and systematic tool to investigate the growth mechanism and a highly controllable means to directly grow nanowires with accurate control of multiple parameters, hence offering considerable advantages compared to conventional furnace process. In Chapter 3, motivated by the fast localized heating capability of laser enabling high temporal resolution, a detailed investigation is carried out on the mechanism of laser-assisted growth of SiNWs such as catalyst diameter- and temperature dependence of nucleation time and catalyst diameter dependence of activation energy of the diffusion of silicon through solid Au.

3.1 Overview

Silicon nanowires (SiNWs) have been very extensively studied due to their high comparability with CMOS-based technology and the possible integration into future devices. To date, the Vapor-Liquid-Solid (VLS) growth mechanism has been considered as a very promising fabrication method for nanoscale-synthesized materials such as nanotubes and nanowires since 1960s' introduced by Wagner and Ellis³³. since high aspect ratio can be achieved without conventional lithography processes. During the VLS growth, vapor Si is preferentially incorporated at the surface of a metal catalyst, diffused through it, and then precipitated at the interface of a catalyst droplet and silicon after the supersaturation of Si in a metal droplet. Continuous incorporation of Si into the droplet results in the growth of a SiNW.

To realize SiNWs-based devices, many studies have been carried out to understand and control the growth of SiNWs using ex-situ and in-situ techniques. Schmid *et al.* found the growth direction depends on the size of a catalyst competing

between solid-liquid interfacial energy and vapor-liquid surface energy with theoretical model and experimental results.⁵⁹ Cui *et al.* showed that the diameter of the grown SiNWs strongly depends on the catalyst size.⁶¹ Kikkawa *et al.* found that the growth rate also depends on the catalyst size.⁵¹ While issues related to the dependence of growth rate on the size of a catalyst have sparked considerable debate, the nucleation time has been also importantly observed by Kalache *et al.*⁶² However, since SiNWs have been mostly grown under furnace or substrate heater, it is not sufficient to observe the very early stage of the growth with high temporal resolution. *In-situ* transmission electron microscopy (TEM) has been also applied to observe VLS driven nanowire growth, but the level of gas pressure is much different than real growth conditions implemented in a furnace environment.

The purpose of this work is to present a detailed investigation on the growth mechanism with high temporal resolution. Especially, the nucleation time and growth rate dependence on the size of a catalyst are studied. To achieve this, a focused laser beam is introduced by a heating source. We have recently introduced a laser assisted technique as not only a convenient and systematic tool to explore new types of nanostructure growth mechanism, but also a highly controllable mean to directly grow nanowires at arbitrary position accuracy and superb dimensional control. As shown in the study, the fast local heating capability of focused laser on O (10-100 μ s) provides high enough temporal resolution allowing exploration of the growth mechanism from the very early stage of the growth, compared to reported studies. Another purpose is to investigate the mechanism of the fast growth of SiNWs. Surprisingly, not any study has been performed to our knowledge that describes fast growth of SiNWs.

3.2 Experimental Setup

Figure 3-1 shows a schematic diagram for laser induced local SiNWs growth system. Poly-L-Lysine was coated on 4.5 μ m thick amorphous silicon film sputtered on the fused silica substrate and then one of size-calibrated colloidal AuNPs (50 and 100 nm in diameter) spread and then was incubated for 7-8 minutes. Since negatively charged AuNPs are attached to positively charged Poly-L-Lysine film, electrostatic interaction between them immobilizes AuNPs. After the assembly, the sample was cleaned by oxygen plasma etching (power = 50 W, O₂ flow rate = 50 sccm, etching time = 1 min) to remove all organic materials including Poly-L-Lysine. Continuous wave (CW) Ar-ion laser at a wavelength of 514.5 nm was focused through the substrate at the interface of amorphous silicon film and fused silica substrate on a spot of diameter 5 μ m at the 1/e²-point. To simulate furnace based SiNWs growth environment conditions with the exception of maintaining localized growth by laser, the film was sufficiently thicker than the optical penetration depth (170 nm measured

by ellipsometer) at the wavelength of the laser, which minimizes direct Au catalyst heating and guarantees sufficient absorption of energy from laser by the film. For controlled gas environment, the sample was enclosed within a vacuum chamber that had two optical windows allowing laser access from the substrate side of the sample and *in-situ* monitoring of laser assisted growth by reflection optical microscope from the film side. 0.9% SiH₄ diluted in He was introduced into the reaction vacuum chamber at 200 sccm maintaining 6.5 Torr as a partial pressure of SiH₄ (P_{SiH_4}) set at relatively high partial pressure due to limited SiH₄ gas concentration. To investigate the very early stage of the SiNW growth, laser illumination time was varied in the range of 10 ms – 30 s by a mechanical shutter. Laser power was controlled by an attenuator consisting of a half-wave plate and a polarizing beam splitter and monitored in real time via the beam reflected out of a polarizing beam splitter. The samples were analyzed by scanning electron microscope (SEM).

3.3 Experimental Results & Discussion

Figure 3-2 shows representative images of SiNWs directly grown on an amorphous silicon film of a single platform by a focused laser. For this growth, 100 nm AuNP was assembled on the film and laser illumination time was varied from 1 to 30 s for different growth time. Laser power corresponding to the growth temperature with assumption of linear dependence was varied from 20 to 45 mW. Figure 3-3 shows the length of SiNWs as a function of laser illumination time measured from Figure 3-2. The growth rate ranging from 200 nm/s (20 mW) to 607 nm/s (40 mW) and is two to three orders of magnitude greater than reported using the conventional furnace process.^{59,60} Especially, compared to the experimental data (~10 nm/s at maximum) of Kikkawa *et al.*⁵¹ investigated at similar gas conditions (1% diluted SiH₄ gas held at 98 kPa), laser-assisted local growth technique achieved one order of magnitude faster growth rate although the flow rate was about 7.5 times lower than 1500 sccm of Kikkawa *et al.* A possible reason is that the great growth rate comes from different diffusion path of a gas between point-like, locally confined CVD and conventional large-area CVD. Bäuerle has already discussed the laser chemical vapor deposition (LCVD) technique of several materials.⁶³ He reported in the study that the rates are several orders of magnitude faster than conventional CVD large-area flow and argued that since the reaction occurs at the localized hot spot created by the laser on the substrate, three-dimensional diffusion path of gas is effectively open for local reaction zone rather than one dimensional path such as for conventional furnace CVD technique, resulting in abundant supply of gas into the reaction zone.

3.3.1 Fast nucleation of laser-assisted growth of silicon nanowires

In Figure 3-3, the growth is respectively initiated at 1 and 3 s for laser power of 25-40 mW and 20 mW. It is found from this result that the apparent growth occurs with a certain temporal delay that depends on the applied laser power level. It is noted, however, that in the present study minimum time step was 1 s. In the VLS mechanism, with increasing temperature, a Au catalyst becomes liquid alloy with silicon in vapor phase which is favorably adsorbed at the surface of a Au catalyst. Due to the concentration gradient at the surface, silicon diffused through the liquid alloy droplet. After reaching a critical concentration of Si at the liquid-solid interface, Si starts to be precipitate, followed by actual growth of SiNWs via continuous Si precipitation. Therefore, some delayed time at the early stage is expected for the apparent growth of SiNWs. Many efforts to investigate the delayed time at early stage of the growth have been made by other groups using *in-situ*^{64,65} and *ex-situ*^{62,66} observations. It was observed in their experimental results and theoretical analysis that the growth of a SiNW doesn't occur instantaneously. Instead, a specific time was required for the actual growth to occur which is called the nucleation time. Although their efforts observed the temperature dependence of the nucleation time, it does not seem to be easy to exactly investigate the nucleation time for laser-assisted fast growth of SiNWs because of the quite different partial pressure level for the growth or insufficient temporal resolution.

In the present study, on the other hand, the growth time was controlled by O (1 ms) at minimum time step for a detailed investigation from very early stage for the laser-assisted fast growth because the minimum temporal resolution corresponds to fast localized heating on O (10-100 μ s). The nucleation time was obtained again in the experiment wherein the growth time and laser power corresponding to the growth temperature were varied from 0 to 3 s and 25 to 45 mW, respectively. In Figure 3-4, scanning electron microscope (SEM) images show very early stage of SiNW synthesis. Figure 3-4(a), (b), (c), and (d) correspond to laser-assisted local CVD runs with fixed power of 45 mW at 8, 10, 20, and 100 ms, respectively. In this experiment, it is readily confirmed by laser-assisted that nucleation occurs at the droplet edge as investigated by Kim *et al.*⁶⁵ and Hofmann *et al.*⁶⁷ using *in-situ* TEM, which implies that supersaturation is needed for nucleation. The growth of SiNWs occurs between 8 ms and 10 ms so that the nucleation time was chosen to be 9 ms. Once the growth of SiNWs starts, they are steadily grown as shown in Figure 3-4(d). A similar calculation of the nucleation time was applied for other temperatures (laser powers). It is presented in Figure 3-5 that the nucleation time ranges between 8 to 175 ms for laser-assisted local growth of SiNWs from 50 nm AuNPs, which is in good agreement with experimental and theoretical study of Kalache *et al.*⁶² However, it is apparently found that the nucleation time is in the three orders of magnitude lower range than that of a

previous report discussing the 15 s to 180 s.^{62,51} A possible explanation for the difference is primarily different diffusion mechanism of a reactant gas. It is recalled that the growth rate is two to three orders of magnitude faster for laser-assisted growth than for conventional furnace growth, which follows the same trend as the nucleation time. For laser-assisted growth, therefore, it is believed that 3-D diffusion of SiH₄ gas into the local reaction zone can significantly shorten the nucleation time. Another possible reason is different morphology of the Au catalyst before the growth. Since colloidal AuNPs are used for this study, there is no time needed to form the catalyst from an evaporated Au thin layer as a catalyst. This may in fact enable more exact estimation of the nucleation time starting from the incorporation of Si vapor at liquid-vapor surface.

3.3.2 Catalyst size- and temperature-dependence of nucleation time

Figure 3-6(a) shows the nucleation time with respect to different catalyst sizes with varied laser power from 25 mW to 45 mW. It is shown in Figure 3-6 that the nucleation time decreases in exponential fashion with temperature at the same catalyst size, which is in good agreement with Kalache *et al.*'s experimental and theoretical study.⁶² Such dependence of nucleation time can be explained by Fick's second law of diffusion by simplification of the geometry in one dimension with a moving boundary of the liquid-solid interface.

One dimensional transient diffusion equations:

$$\begin{aligned} \frac{\partial c_L(x,t)}{\partial t} &= D_L \frac{\partial^2 c_L(x,t)}{\partial x^2}, & 0 \leq x \leq x_0(t), \\ \frac{\partial c_S(x,t)}{\partial t} &= D_S \frac{\partial^2 c_S(x,t)}{\partial x^2}, & x \geq x_0(t), \end{aligned} \quad (1)$$

$(D_S \ll D_L)$

Boundary conditions:

$$\begin{aligned} c_L(0,t) &= c_{L0}, \\ c_L(x_0,t) &= c_1 = c_S(x_0,t) = c_1, \\ c_S(x,0) &= 0, \end{aligned} \quad (2)$$

where D_L and D_S are the diffusion coefficients of silicon through liquid and solid gold, c_L and c_S the silicon content of the liquid and solid phase, and $x_0(t)$ the moving liquid-solid boundary, respectively. By assuming d is the height of the nanoparticle and continuity of the silicon flow at the interface of liquid-solid, the nucleation time is :

$$t \approx \frac{d^2}{D} \approx \frac{d^2}{D_0 \exp\left(-\frac{E_a}{KT}\right)} \approx \exp\left(\frac{E_a}{KT}\right) \quad (3)$$

In Figure 3-6(a), size effect of nucleation is also displayed. Larger catalysts show longer nucleation time as expected from scaling arguments.^{64,67} According to Gibbs-Thomson effect, in addition, supersaturation decreases as a function of the catalyst size.

$$\Delta\mu = \Delta\mu_0 - 4\Omega\alpha/d$$

where $\Delta\mu$ is the effective difference between the chemical potentials of Si in the vapor phase and in the catalyst, α is the specific free energy of the catalyst surface, Ω is the atomic volume of Si, and d is catalyst diameter. However, it is significantly found in this experiment that the ratio of the nucleation times corresponding to two different catalyst sizes (100 nm and 50 nm) increases with decreasing temperature. Herein, it should be noted that eutectic melting temperature of Si-Au is size-dependent as melting temperature of gold nanoparticles (single system) is.⁶⁸ Wautelet *et al.* has theoretically studied that eutectic melting temperature is size-dependent and suppressed for smaller particles.^{69,70} More recently, several groups have experimentally reported changes in fundamental phase diagram of nanoscale small particles used for vapor-liquid-solid growth due to intrinsic size effects.^{71,72} Therefore, it is believed that a larger catalyst requires higher temperature to efficiently reach supersaturation for nucleation. Accordingly, due to the size effect supersaturation occurs at lower temperature, near the eutectic temperature rather than at the higher temperature predicted by the equilibrium phase diagram.

3.3.3 Catalyst size dependence of activation energy

In Figure 3-6(a), the nucleation times are plotted as a function of the inverse of power in a semi-logarithmic scale. Considering the assumption of linear dependence of temperature on power and eq. (4), the slope represents the activation energy of the diffusion of silicon through solid Au. From two slopes, activation energy is size dependent and increases with the catalyst size. It should be noted that lower activation energy shorten the nucleation time. Moreover, since it is also earlier shown that nucleation time decreases with shrinking the catalyst size, it is also believed that activation energy decreases with catalyst size. From the plot of nucleation time with respect to the inverse of estimated temperature in Figure 3-6(b), it is found that the activation energy ranges between 0.78-1.06 eV (75-102 kJ/mol) for 50 ~ 100 nm in diameter. Since this range is higher than Kalache *et al.*'s value (0.68 eV)⁶² using smaller particles (< 50 nm in diameter) and is relatively lower than that of the

diffusion of Au through Si(1.13 eV),⁷³ it is believed that the activation energy observed in this study is valid for VLS growth mechanism.

3.3.4 Branched growth of SiNWs

Figure 3-7 shows SEM images of SiNWs grown from 100 nm AuNPs for 20 s and 30 s with fixed laser power of 25 mW. Compared to growth from 50 nm AuNPs, it is observed that branched small diameter SiNWs are grown at the base of the large SiNWs from 100 nm AuNPs. The branched growth of small SiNWs can be explained by recalling the concept of critical diameter which has been reported by Givargizov.⁷⁴ More recently, Dhalluin *et al.* has reported of the P_{SiH_4} dependent critical radius for growth of SiNWs.⁷⁵ It was found in the study that the density of small diameter SiNWs grown from the sidewall of a SiNW trunk increases with increasing P_{SiH_4} . As discussed previously in section 3.3.2, the supersaturation inversely depends on the catalyst size. By assuming that increase of P_{SiH_4} leads to an increase of the supersaturation in silicon of the Au-Si droplet, therefore, it is believed that under high P_{SiH_4} favorable for growth of small diameter SiNWs, a large catalyst produces branched small SiNWs as shown in Figure 3-7. Incidentally, the branches in this study are at the base of large SiNWs, unlike branches of SiNWs that as Dhalluin *et al.* showed grew from small Au droplets that diffused along with the sidewall of SiNW trunks. Considering this, we focused more on the early stage of growth from 140 nm AuNPs. It is shown that at growth time of 1 s (Figure 3-8(a)) thin hairs decorates the surface of the droplet edge that is a site of heterogeneous nucleation. At 2 s (Figure 3-8(b)), a small branched SiNW appears at the base of trunk as well as tiny Au droplets on its sidewall. Laser-induced sudden heating can cause instability of the liquid droplet due to the steep surface tension gradients imposed by the confined temperature distribution. Wagner *et al.* has observed branching caused by sudden increase in temperature which was intentionally made in the experiment.⁷⁶ The volume of the droplet increases with sudden increase of temperature, which possibly causes an unstable contact angle configuration in VLS. Stable contact angle configuration is mediated by force balance at the solid substrate/droplet/vapor interface. It is believed that tiny Au droplets can be formed at the liquid droplet forms, consequently presenting nucleation sites for the branched small SiNWs under favorable P_{SiH_4} condition favored for growth of small SiNWs. According to the experimental results and previous reports, it is pointed out that P_{SiH_4} should be lower to decrease or prevent branches of small SiNWs,

3.4 Summary

In this chapter, very early stage of growth of SiNWs could be precisely dialed with temporal resolution of 1 ms by taking faster localized heating capability of laser, compared to conventional furnace process. It is even believed from the experimental results that laser-assisted technique with high temporal resolution can serve to facilitate *in-situ* observation technique since it can be carried out under the same partial pressure level of reactant gases as conventional furnace process is. For laser-assisted growth, most of all, it was found that nucleation time is shortened by 2 to 3 orders of magnitude compared to conventional furnace growth. Since laser-assisted growth rate is similarly by orders of magnitude greater than that of conventional furnace growth, it is believed that three-dimensional diffusion effect of precursor gas dominates in the nucleation stage as well as the subsequent growth stage of SiNWs. In this respect, this is the first report investigating the mechanism of fast growth of SiNWs. Further investigations on the early stage mechanism of fast growth showed that the nucleation time depends on the catalyst diameter and growth temperature. It was also found that activation energy for the diffusion of silicon through solid Au is also catalyst diameter-dependent and increases with increasing catalyst diameter. With larger catalysts, it was found that small SiNWs branched at the base of a parent large SiNW due to sudden heating by a laser and P_{SiH_4} condition favoring growth of small SiNWs. From this study, it was confirmed that laser-assisted technique is a systematic tool to explore nano-synthesized materials.

FIGURES

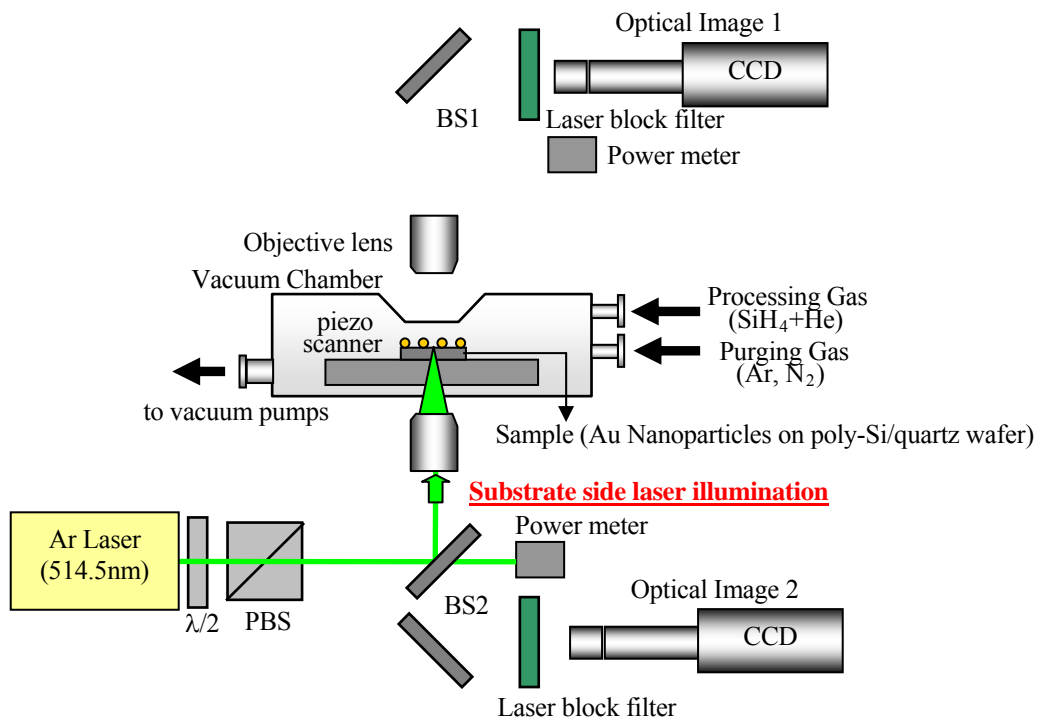


Figure 3-1. A schematic diagram for laser induced local SiNWs growth system.

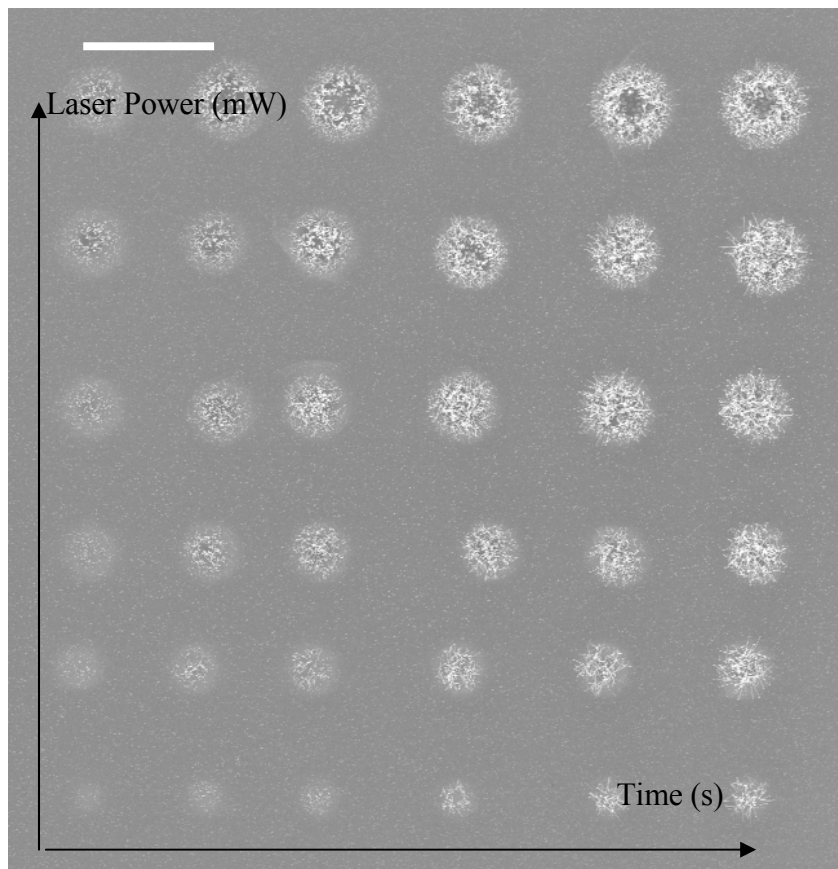


Figure 3-2. Scanning electron microscope image of SiNWs grown from 50 nm AuNPs on a 4.5 μm amorphous silicon film by focused laser of which illumination time was varied from 1-30 s and power from 20 mW to 45 mW. The scale bar in the figure is 20 μm .

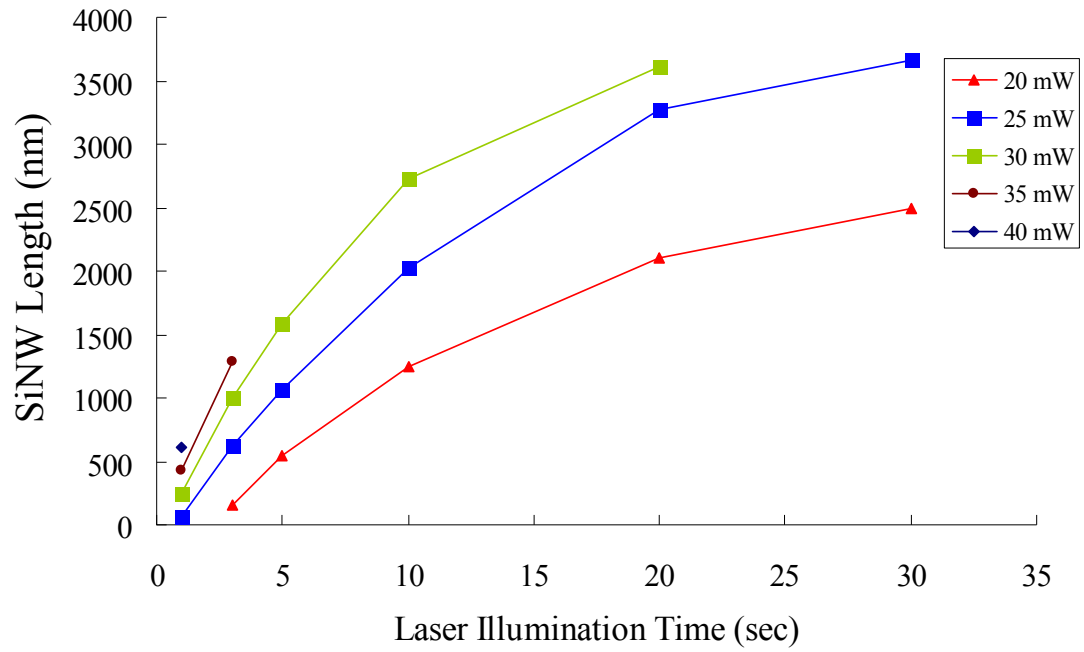


Figure 3-3. The length of SiNWs as a function of growth time at laser power varied from 20 mW to 40 mW which are measured from Figure 3-2.

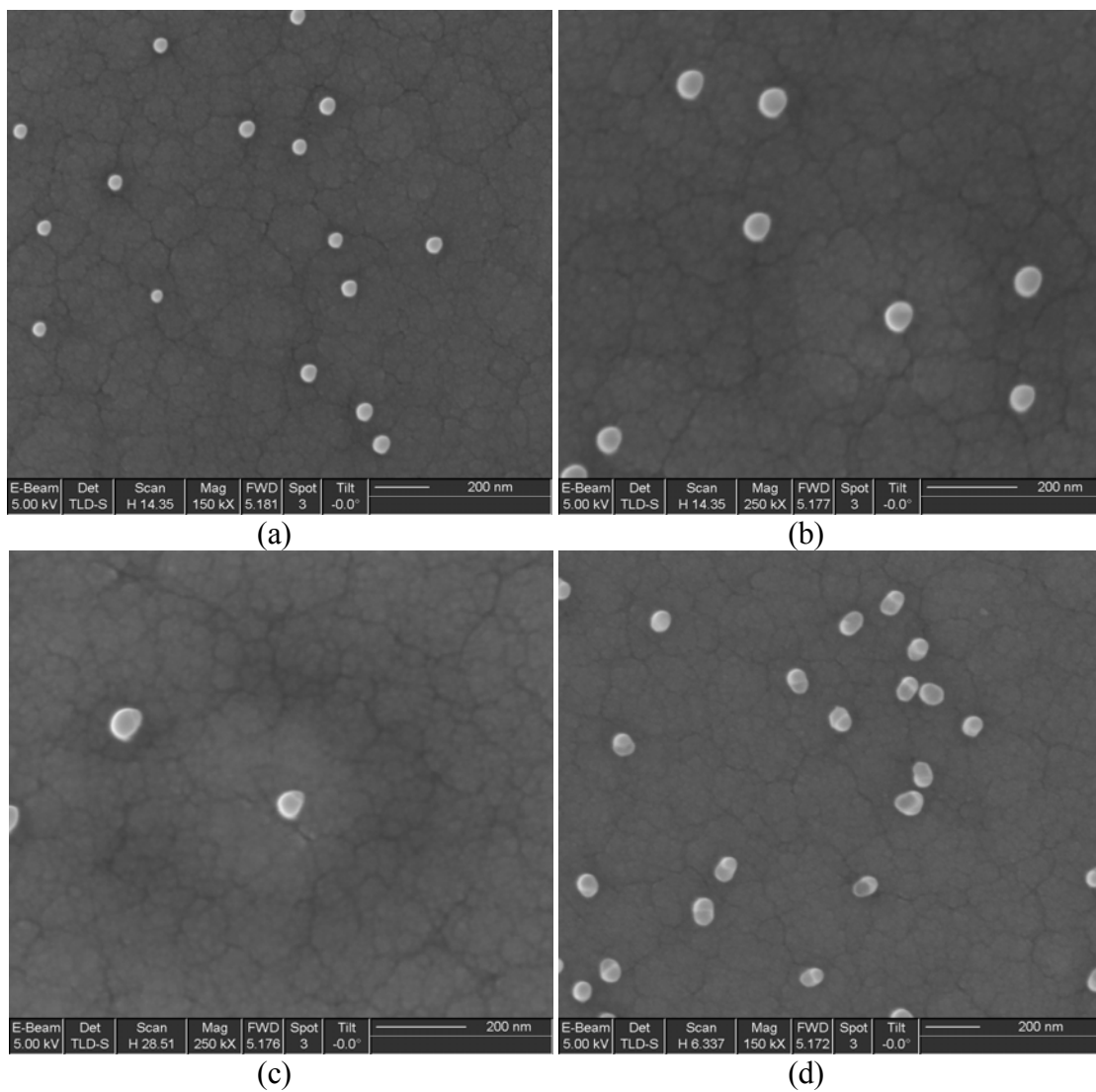


Figure 3-4. Scanning electron microscope images representing the stages just prior to nucleation, 8 ms (a), just after nucleation, 10 ms (b), 20 ms (c), and 100 ms (d) for 50 nm colloidal Au nanoparticles. Laser power was fixed at 45 mW and P_{SiH_4} was maintained at 6.5 Torr with flow rate of 200 sccm.

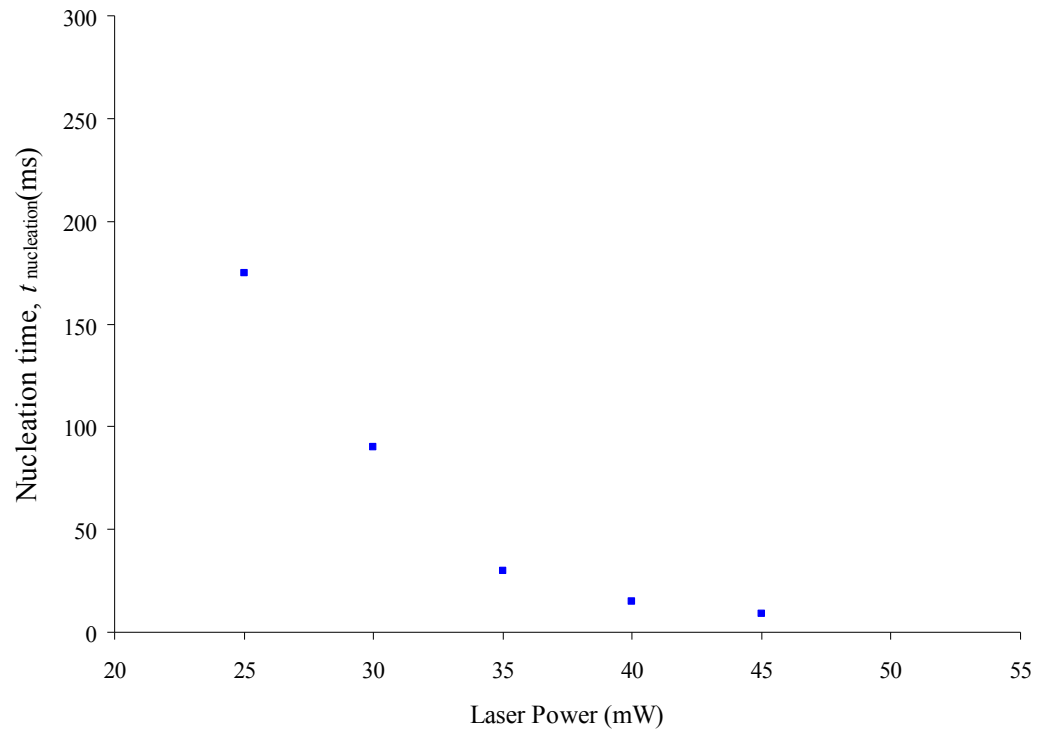


Figure 3-5. Nucleation time measured for laser power from 25 mW to 45 mW.

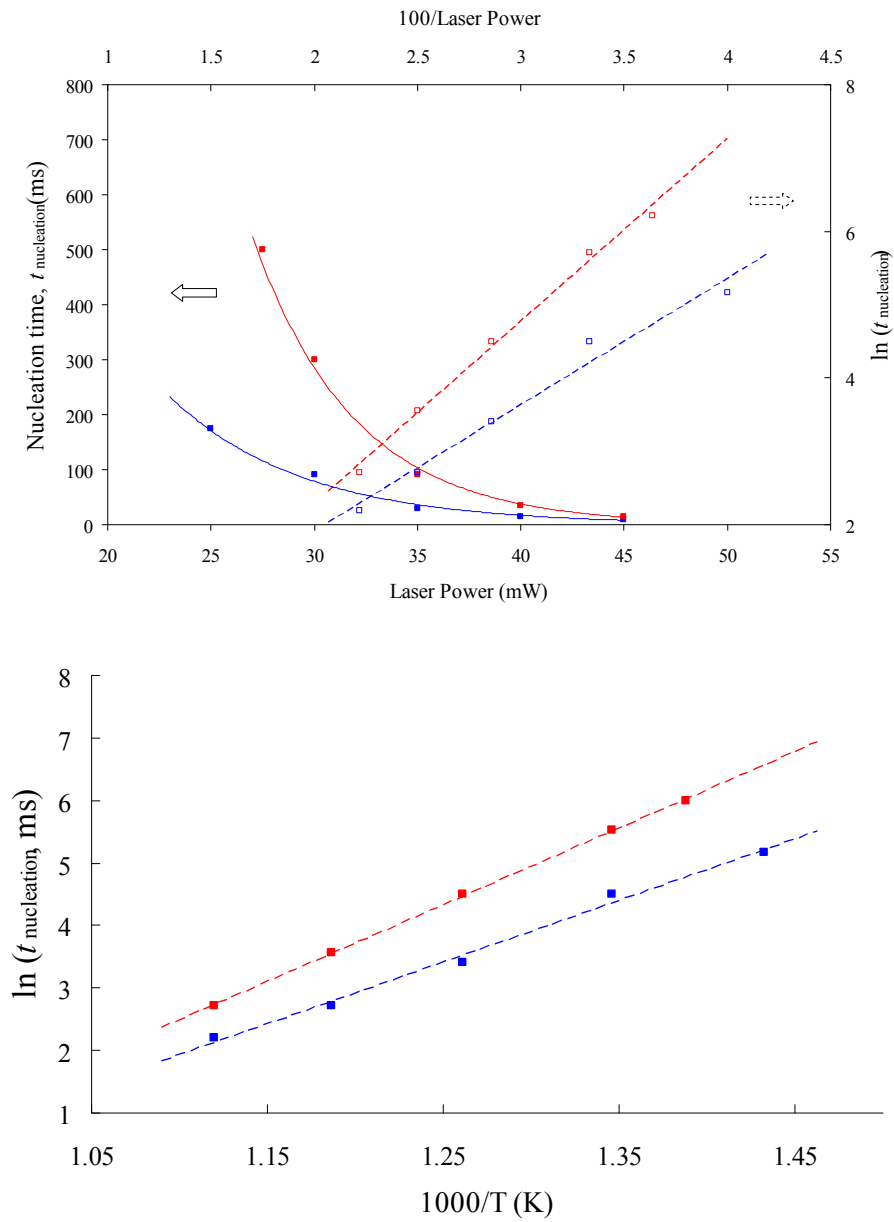


Figure 3-6. The nucleation time with respect to different catalyst sizes (50 nm (blue) and 100 nm (red)) at varied laser power from 25 mW to 45 mW representing the temperature. The nucleation time is a function of the inverse of temperature in a semi-logarithmic scale.

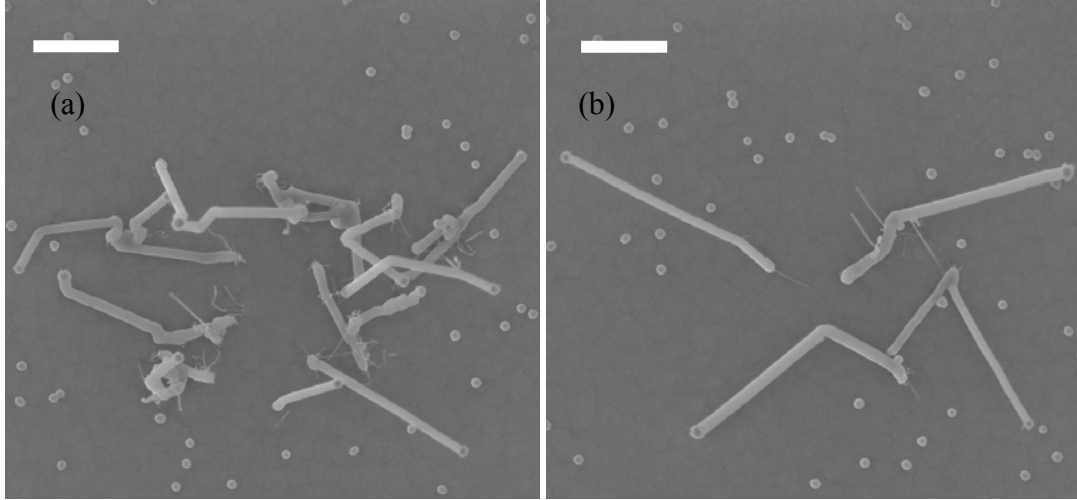


Figure 3-7. Scanning electron microscope (SEM) images of laser-assisted growth of SiNWs with various time at fixed laser power of 25 mW. Au catalysts are 100 nm in diameter. (a) and (b) are for 20 s and 30 s, respectively. The scale bars in the figures are 1 μm .

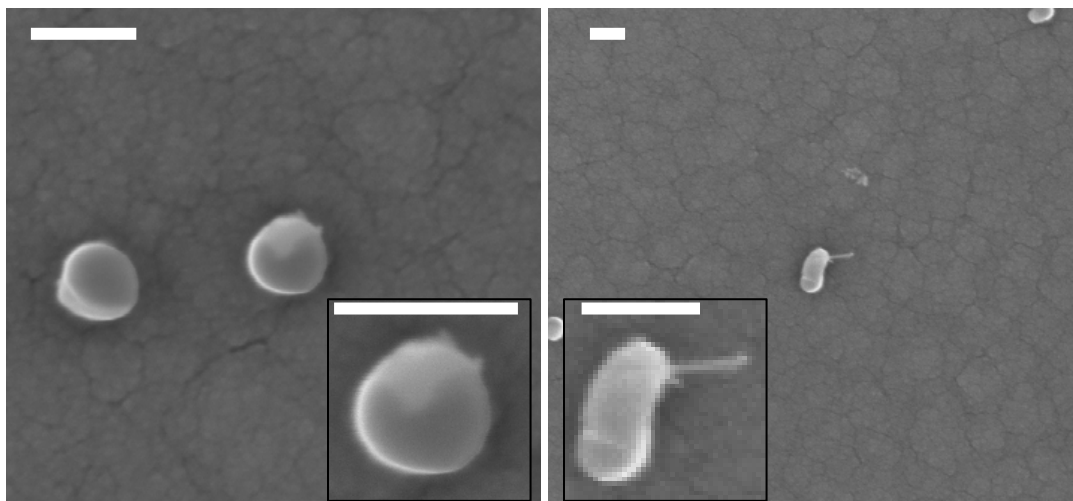


Figure 3-8. Scanning electron microscope (SEM) images representing early stage of growth of SiNWs from 140 nm diameter AuNPs for 1 s (a) and 2 s (b) respectively. Laser power was fixed at 25 mW. The scale bars in the figures are 200 nm.

CHAPTER 4

LASER INDUCED NANOSCALE-SELECTIVE DIRECT GROWTH ON DEMAND BY OPTICAL NEAR FIELD TECHNIQUE

This chapter presents that the direct growth of a single silicon nanowire (SiNW) is grown by employing optical near-field technique. Continuous wave (CW) 514.5 nm laser radiation is confined via an optical near-field probe is confined beyond the diffraction limit and provides direct nanoscale illumination heat source for local growth. Aided by indirect heating of a gold nanoparticle (AuNP) catalysts, the energy of direct laser illumination over AuNPs is minimized, resulting in lowering the local temperature increase. Therefore, heat source with sharp hillcock-like profile rather than the broad Gaussian can be concentrated beyond the diffraction limit, which would favorably enable controlled direct growth of a single SiNW among randomly distributed AuNPs with spacing in nanoscale distance. It is also shown the growth trend is influenced by the beam size of direct laser illumination as well as the local temperature increase of the AuNP absorbed by Mie theory. As a result, this study demonstrates that a laser illumination source confined beyond the diffraction limit in near field could be a versatile tool for the direct growth of semiconductor NWs at pre-specified area with nanoscale selectivity.

4.1 Overview

Semiconductor nanowires (NWs) have attracted great interest as promising materials for the future generation devices such as nano field effect transistors,^{9,77,78,79,80} optoelectronics,^{45,44} resonantors,³¹ biosensors,^{8,27,81,82} energy conversion and energy storage^{21,17,83,84} due to their good optical and electrical properties. Since synthesis of semiconducting NWs has been generally carried out in an environment of high temperature over the entire substrate, intricate post assembly steps of NWs to the pre-existing structure have been required to prevent damage, although the yield is low. In order to resolve this limitation and even though considerable efforts have been devoted on the compositional and orientation control in

NW growth, the post assembly step by optical and optoelectronic tweezing are not yet sufficient to allow high spatial and angular resolution.^{34,35}

As an efficient path towards this goal, several research groups have demonstrated localized direct growth of SiNWs^{36,37} and CNTs^{38,39,40,41,42} by laser illumination. Since the spatial Gaussian profile of the laser beam can be employed to constrain the lateral size of the reaction zone to dimensions smaller than the actual beam size due to the reaction temperature threshold, it is not surprising that the laser has been considered as a special tool for micro- and nano-fabrication over several decades.⁴⁸ In the growth process of SiNWs, Au nanoparticles have been normally used as catalysts. Herein, under laser illumination, the Au nanoparticle acts as light absorbing material naturally enabling highly localized heat generation within its volume.^{55,85} Furthermore, surface plasmon resonance (SPR) may enhance the absorption efficiency.⁸⁶ This fact has been extensively employed in studying direct nanopatterning^{87,88} and biological sensing applications.^{89,90} Lately, Cao *et al.* employed the localized growth of SiNWs with assistance of SPR due to the direct illumination of far field focused laser over gold nano-catalysts.³⁷ However, it doesn't seem that plasmon assisted synthesis is sufficiently robust for the controlled growth of semiconductor NWs, yet. As also discussed in chapter 2, while direct heating of catalysts which is favorable for localized heating of the catalysts via plasmonic resonance allowed one-dimensional growth at very early stage, the structure deviated from the desired nanowire due to secondary Si deposition on the pre-grown nanowire. On the contrary, indirect heating enabling stable heating of the catalysts through the locally heated substrate showed the laser induced growth kinetically follows the conventional growth trend. However, substrate-side laser illumination to approach indirect heating of catalysts still tends to restrict somewhat applications and the local growth area was limited by the diffusion distance across the film thickness.

In this chapter, it is shown that continuous wave (CW) laser radiation in conjunction with optical near-field probe enables highly selective and stable growth of nanowires among randomly distributed catalysts, compared to far-field direct illumination focused by objective lens. The lateral temperature profile of the substrate and local temperature increase of AuNP were calculated by finite difference time domain (FDTD) and Mie theory, respectively.

4.2 Experimental Setup

Figure 4-1 shows a schematic diagram for optical near-field thermal triggered nanowire growth system in controlled nanoscale area. As a photo-thermal conversion layer, the 2 μm thick amorphous silicon film was sputtered on the fused silica substrate before 30 nm colloidal gold nanoparticles (Ted Pella Inc.) were assembled

on it. The film was sufficiently thicker than the optical penetration depth of the wavelength (514.5 nm) of the laser in order to minimize direct heating of gold nanoparticles (AuNPs) and simultaneously guarantee sufficient absorption of energy from laser by the film. For controlled gas environment, the sample was enclosed within a vacuum chamber which had two optical windows allowing laser beam access both from the bottom- and film- side of the sample. The vacuum chamber was also designed for an optical near-field probe to precisely approach to the sample and be coupled with the film-side illuminated laser. A laser beam in conjunction with the AFM tip plays a role of nano-scale illumination source by maintaining the distance between the top surface of the sample and the AFM tip apex in near-field range of 100 nm. 0.9% SiH₄ diluted in He was introduced into the reaction vacuum chamber at 200 sccm maintaining 6.5 Torr as a partial pressure. Ar⁺ continuous wave (CW) laser was used at a wavelength of 514.5 nm in the experiment. Laser illumination time was varied in the range of 1–30 s by a mechanical shutter. Laser power was controlled by an attenuator consisting of a half wave plate and a polarizing beam splitter and monitored in real time via the beam reflected off the polarizing beam splitter.

4.3 Theoretical Basis

4.3.1 Local temperature of a gold nanoparticle by surface Plasmon

As our previous study explored laser-assisted silicon nanowire growth mechanism, scanning electron microscope (SEM) images in Figure 4-2(a) and 4-2(b) show the growth trends by indirect and direct laser heating of catalysts is intrinsically different. Although film-side laser illumination was favorable for localized heating of catalytic AuNPs by strong absorption due to SPR, it was very difficult to achieve reasonable one-dimensional (1-D) nanowire growth except the very early stage because laser absorption dynamically changes due to local temperature, phase, and shape of Au catalysts and pre-grown nanowires. The effect of direct laser absorption by the catalysts is not negligible in the film-side illumination since local temperature of Au catalysts governs the growth of SiNWs. Laser-induced temperature increase in the particle at steady state is calculated by balancing source (absorption) and loss to the surrounding medium. Main loss is through convection, safely neglecting radiative loss and conductive loss through the substrate due to high contact resistance.⁵⁵

$$\Delta T = T_p - T_m = \frac{I_0 Q_{abs} \pi r_p^2}{h(4\pi r_p^2)}$$

where T_m is the temperature of the surrounding medium, I_0 is the laser irradiation power density (W/cm²), h is convective heat transfer coefficient, and Q_{abs} (~0.5 for 30

nm AuNP at $\lambda = 514.5$ nm) is absorption efficiency by Mie theory. An estimate of the value of convective heat transfer coefficient is approximated from $h \sim k_m/r_p$ where k_m is thermal conductivity of the surrounding medium, by assuming that the heat transfer between the particle and the surrounding medium is dominated by conduction. The thermal conductivity of helium as the surrounding medium is taken to be 0.15 W/mK. For a 30 nm AuNP we used in this study, h is taken to be $O(10^6)$ W/m²K and then local temperature increase by a AuNP is approximated at 10 K for helium environment which can be interpreted as the maximum amount of heating in addition to the base heating from the silicon film, demonstrating the effect of SPR^{36,37} in the growth of nanomaterials. With this additional amount based on our calculation, the local temperature should be still in range for 1-D growth regime. However, laterally grown SiNWs in Figure 4-2(b) imply that real local temperature of Au catalysts may be higher than its calculated value. Herein, it should be noted once Au catalyst reaches the reaction temperature by the add-up amount, the catalyst becomes molten phase of Au/Si mixture. This possibly means that during actual growth process local temperature and/or molten phase of Au/Si mixture will dynamically modify the absorption characteristics resulting in increased local temperature of Au catalysts favoring lateral growth rather than axial growth. The presence of conical shaped SiNWs in Figure 4-2(b) apparently indicates that the temperature gradient within nanowires was formed from Au catalytic sites to the substrate and the lateral growth dominantly showed up near Au catalysts, not uniformly along with grown SiNWs. Therefore, reasonable growth of nanowires could be attained only at very early stage and thereafter rapidly followed by secondary lateral Si deposition.

4.3.2 Direct laser absorption on grown silicon nanowires

Additional absorption onto the initially grown portion of the SiNWs may also lead to secondary direct CVD on the nanowire surface. Misra et al. showed that the absorption of laser light in SiNWs is strongly dependent on the light polarization and diameter.⁵⁶ By employing finite difference time domain (FDTD) simulation, absorption efficiency for a SiNW with 30 nm in diameter is lower by 1 and 2 orders of magnitude, respectively, along and normal to the polarization (electric vector) than the efficiency of a AuNP of the same diameter. Via the above mentioned procedure for AuNPs, the calculated local temperature increase of grown SiNWs aligned normal to light polarization is approximately 0.1 K, which is negligible with respect to that of AuNPs. Although the diameter of the SiNWs can lead to different absorption efficiency, it is not meaningful to expect temperature increase sufficient for lateral growth since grown SiNWs still remain in solid phase. Therefore, it is possibly

postulated that the minimization or the prevention of direct illumination of laser in Au catalysts would promote controlled 1-D growth SiNWs in localized area of interest.

4.4 Experimental Results & Discussion

One of methods to decrease the direct laser absorption in Au catalysts is to increase the base temperature of the substrate as well as Au catalysts in advance, which should be below the eutectic temperature (363°C) of Au-Si binary system to prevent the chemical reaction. This enables film-side laser illumination to play a role of trigger growth of SiNWs with minimal power inducing lower local temperature increase (ΔT) of AuNPs as discussed earlier. Therefore, it is expected to reduce the dynamic change of the local temperature caused by molten phase of Au-Si mixture and to grow SiNWs in better controlled way. Although blanket substrate heating and localized heating of interest can be considered as a supportive or assisting heating, the latter by substrate-side laser illumination was preferred for the experiment to achieve tighter heat confinement and faster heating of O ($10\text{-}100\ \mu\text{s}$) as will be discussed later.

SEM images in Figure 4-3 show SiNWs grown under film-side laser illumination (for direct heating of catalysts) with assistance of substrate-side laser illumination (for indirect heating of catalysts). Substrate-side laser focused by 10X objective lens was continuously illuminated at 72 mW in advance to elevate the local temperature of interest as near as possible the reaction temperature, which confirmed no growth reaction by itself. By adjusting the laser power and varying illumination time of film-side illumination, the SiNWs became grown by $2\text{-}3\ \mu\text{m}$ without striking lateral growth or secondary CVD at 2 mW for 30 s and 3 mW for 20 s as shown in Figure 4-3(a) and 4-3(b), respectively. Laser power of film-side illumination is apparently lowered by one order of magnitude with assistance of a supportive heating compared to that of pure film-side laser illumination. Therefore, with the local temperature increase (ΔT) driven by direct laser absorption lowered by estimated value of 0.5°C , SiNWs are grown in 1-D under more precise control of the temperature by certain length and time as shown in Figure 4-3(a) and 4-3(b). At 3 mW and 30 s, however, lateral growth or secondary Si CVD appeared on pre-grown nanowires resembling inverse conical shape, again as shown in Figure 4-3(c). In Figure 4-3, since molten Au nanoparticles and growing nanowires during the growth are within laser light affected zone by direct illumination whose size is several microns. It appears that the dynamical variation of laser absorption depending on a number of factors such as phase and geometry of the Au catalysts and absorption/heating on the growing nanowire stem still causes unstable growth. In this result, it is shown once more how narrower the growth processing or temperature window becomes for controlled axial growth under direct laser illumination.

Therefore, in addition to supportive heating, it seems to be more desirable that direct laser coupling with the Au catalysts as well as with the pre-grown nanowires should be minimized during the growth process.

As previously argued, the temperature profile is broadened by the laser focal spot roughly by factor of 2 (effective diffusion length of r_{laser} at steady state) and the broadened Gaussian-like temperature profile incurs growth spot size smaller than the laser focal spot size through precise control of threshold laser power for the growth reaction. The size of growth spot can be further reduced by use of tighter focus or optical near-field,⁵⁸ resulting in reducing laser light affected size. SEM images in Figure 4-4 depict SiNWs grown under near-field focused film-side laser illumination with various illumination time and laser power. Since the film-side illuminated light in conjunction with a typical silicon nitride AFM tip is spatially confined below the diffraction limit, it can serve as nano-scale illumination source by maintaining the distance between the top surface of the sample and the AFM tip apex at 100 nm. The substrate-side laser local heating necessarily assisted the experiment as in far-field focused film-side laser illumination for the same purpose. It is observed that SiNWs were selectively grown without striking lateral growth or secondary direct Si CVD under the near-field laser illumination, compared to that of far-field focused film-side laser illumination. At 3 mW of input laser power for 30 s, only a single Au catalyst was reacted among random distributed AuNPs on the substrate in Figure 4-4(a). This nanowire was mainly kinked during the growth possibly due to lower power or growth temperature. With increasing input laser power by 4 mW for 20 s, two Au catalysts within the film-side laser illumination area were activated yielding 1-D growth of SiNWs as shown in Figure 4-4(b). The result shows that nanoscale illumination light source has excellent controllability and selectivity enabling the growth of a single SiNW to multiple SiNWs by adjusting the laser power. Therefore, it is postulated that there are several possibilities for growing 1-D SiNW by near-field illumination source. One possibility may come from the markedly reduced laser illumination area. Once the Au catalyst is activated to produce a SiNW, it can instantly escape from the nanoscale light-affected area and be controllably grown in 1-D by heat conduction from the root to the catalyst without any influence of the laser light. However, this scheme is more appropriate for inclined or horizontally grown SiNWs rather than for the vertically grown ones. Another one is the indirect heating of AuNPs even under film-side illumination. This possibility has already been observed in pure film-side laser illumination shown in Figure 4-2 (b). Since the rim of the growth reaction area was determined by lateral heat diffusion through the a-Si film and fused silica substrate underneath AuNPs, several AuNPs in that area could be activated without direct absorption from the beginning stage. However, this indirect heating of AuNPs was very limited in the rim of the micron-sized beam, which eventually showed no more than mixed growth reaction as shown earlier. On the other hand, near-field

focused illumination utilized in this study could be located in the vicinity of the AuNPs at a spacing of hundreds of nanometers and drive localized growth of a single SiNW in nanoscale area. This is beyond the limitation of far-field direct illumination as shown earlier. SPR effect also possibly plays an important role of the selective growth as Cao *et al.* demonstrated in their work that this effect helped localized reaction and growth of nanomaterials among surrounding catalysts.³⁷ Several groups explained that localized SPR in the nanoparticle is influenced by the physical environment of the assembled system such as substrate effect, the distance between the nanoparticle and the substrate, the distance among nanoparticles and size, shape and metal composition of the nanoparticle,^{86,91,92} resulting in different absorption efficiency. In this study, moreover, surface roughness of about 10 nm of a-Si film and size variation in AuNPs cannot help causing the different local temperature increase in AuNPs. Therefore, they can be more selectively activated as observed in Figure 4-4(b) showing the particles outside the laser light affected area remained inactive.

For further investigation of thermal confinement effect by near field illumination coupled with assisting substrate-side laser local heating, a detailed temperature profile across the particular material structure consisting of 2 μm a-Si film and 500 μm fused silica was obtained. The numerical analysis of three-dimensional heat diffusion equation considered the volumetric heat source term in the film and radiative/convective losses to the surrounding medium (losses almost negligible). The plasmonic-enhanced absorption effect by nanoparticles was excluded in the first analysis. Steady temperature profile is essentially determined when the laser-induced source terms is balanced with diffuse loss. The time to reach steady state temperature (t_{st}) is roughly scaled as $\sim r_{\text{laser}}^2 / \alpha_{\text{Si}}$ at the surface of a-Si film in the center of the laser spot. Again, convective and radiative losses are minor and can be reasonably neglected (r_{laser} is laser focal spot radius and it is also an effective heat penetration depth at steady state,⁵⁰ and α_{Si} is thermal diffusivity of silicon thin film). The estimated t_{st} then becomes $\sim O(10 \mu\text{s})$ that was also confirmed by our numerical analysis. Computations were carried out to analyze the parameters required for reaching the same peak temperature (400°C) at the top surface of a-Si film and at the center of the laser spot. Film-side laser illumination beam of different size was coupled with substrate-side laser local heating corresponding to 350°C and hence safely below the growth possible temperature of 363°C . Numerical analysis in Figure 4-5 shows that the shape of lateral temperature profile changes from the Gaussian shape corresponding to single beam heating heating. It appears with tightly focused beam ($\lambda/4$ and $\lambda/2$ in diameter), which has a sharp hillcock-like profile superposed to Gaussian-like broader background heat diffusion profile. Due to this modified temperature profile, the reaction size above the threshold temperature of 370°C where growth can occur can be dramatically reduced by about 250 nm in diameter with $\lambda/4$

(~128 nm) size focused beam, compared to 3.8 μm with 10 μm size focused beam. While $\lambda/4$ (~128 nm) size focused beam has growth reaction area composed of the direct heating by film-side laser illumination (< 128 nm) and indirect heating by lateral thermal diffusion in the range of 128 and 250 nm, 10 μm size focused beam always confines the growth reaction just within direct laser illumination. Local temperature increase of AuNPs on a-Si substrate induced by different laser beam size can be calculated by Mie theory as discussed earlier assuming no phase change of the AuNPs. In far-field focused direct laser illumination (1.51 mW at 10 μm in diameter), this merely contributes to the local temperature increase (0.24 $^{\circ}\text{C}$) of solid phase AuNPs with assistance of substrate-side laser local heating. However, the calculated absorption efficiency is not valid once AuNPs are transformed into molten phase of Au/Si catalysts in VLS growth process. In this case, they can be dynamically influenced by light affected area (10 μm) larger than growth reaction area (3.8 μm). Therefore, 1-D pre-grown nanowires eventually experienced lateral growth dominantly originated from Au catalysts with increase of time and/or even a little laser power experimentally shown in Figure 4-3.

On the other hand, tightly focused, beyond the diffraction limit, film-side laser illumination (0.027 mW at $\lambda/4$ in diameter) for a-Si substrate at 400 $^{\circ}\text{C}$ can induce local temperature increase (~60 $^{\circ}\text{C}$) of AuNPs. This is because volumetric heat source reaches a point source inducing improved diffusion loss to the surrounding medium with decreasing laser spot size. This in fact raises the intensity impinging on the nanoparticles by one order of magnitude higher than film-side laser illumination. Even in that high local temperature increase of AuNPs, however, a single or two SiNWs have successfully grown in a controlled sense as shown in Figure 4-4. Presumably the Au nanoparticle does not act as a heat source to continue growing a nanowire any more since very early stage of the growth as upon melting it may escape from the nanoscale laser affected zone. High local temperature increase of the AuNP by direct illumination of nanoscale focused laser can reduce the growth reaction size with decreasing of input laser power. For instance, the AuNP temperature of 400 $^{\circ}\text{C}$ is satisfied with substrate temperature of 373 $^{\circ}\text{C}$ due to direct laser absorption of the AuNP, which allows the growth reaction size to be reduced by about 100 nm in diameter as shown in Figure 4-5.

Blanket heating by a substrate heater can replace the substrate-side laser induced local heating as supportive indirect substrate preheating, minimizing local temperature increase of AuNPs. For numerical analysis, the substrate is considered preheated at 350 $^{\circ}\text{C}$. This value is the same temperature at the center of substrate-side laser local heating. Numerical analysis in Figure 4-6 shows the growth reaction size with respect to focused beam size for film-side illumination among them. The difference apparently stands out with larger focused beam size for film-side

illumination. With the film-side focused beam of 10 μm in diameter, it is shown that laser local preheating can reduce by about half the growth reaction size induced by blanket substrate heating. However, this difference is decreased as the film-side focused beam size shrinks.

4.5 Summary

In this chapter, single AuNP was selectively activated to grow a SiNWa by laser illumination source confined beyond the diffraction limit in near field among randomly distributed AuNPs with spacing in nanoscale distance. To achieve a nanoscaled heat source in this study, a focused laser was coupled with an optical near-field probe. Since it was necessary to protect the probe from heating by laser absorption on its wall, the silicon nitride tip was employed as an optical near-field probe instead of traditional silicon tips. Compared to pure direct heating of AuNPs, the use of assisting indirect heating of AuNPs could minimize the energy of direct laser illumination over AuNPs, resulting in lowering the local AuNP temperature increase. By employing near-field laser illumination, therefore, heat could be more significantly confined since the lateral temperature profile is of sharp, hillcock-like shape rather than the broad Gaussian. As a result, silicon nanowires could be directly grown at a pre-specified position with high nanoscale selectivity. It was also shown the growth trend is influenced by the beam size of direct laser illumination as well as the local temperature increase of the AuNP absorbed that could be predicted by Mie theory.

FIGURES

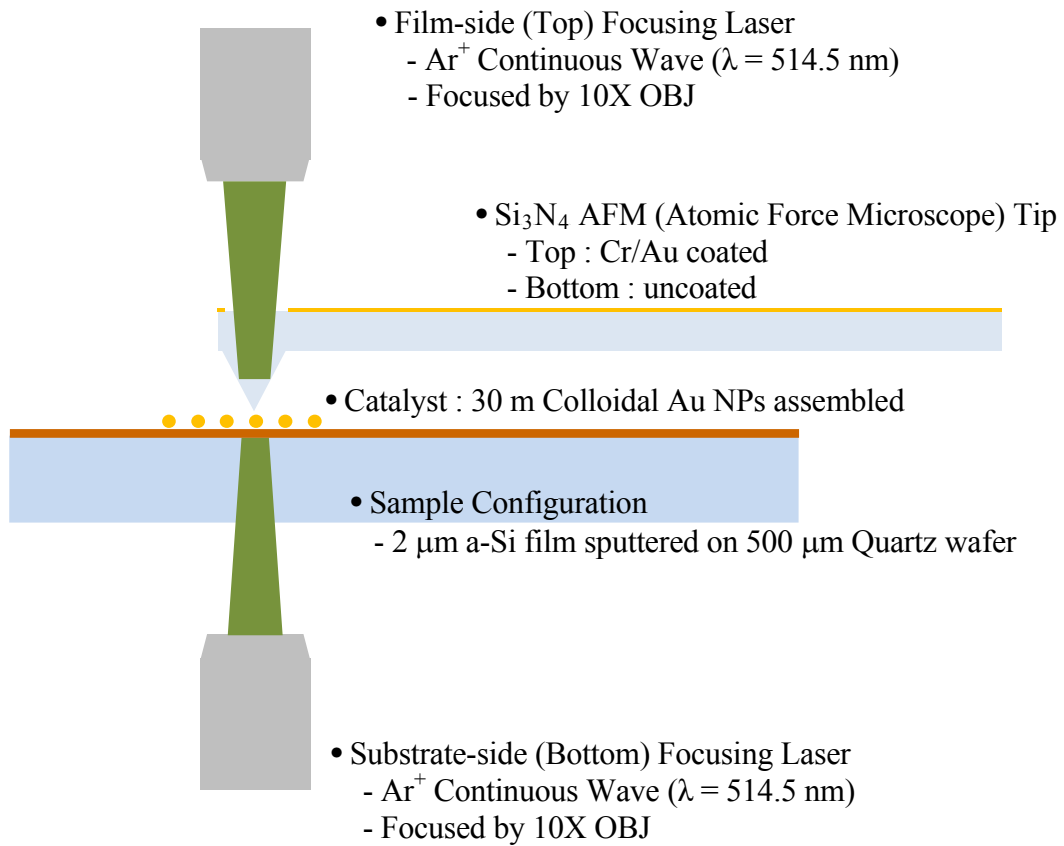


Figure 4-1. A schematic diagram for optical near-field thermal triggered nanowire growth system

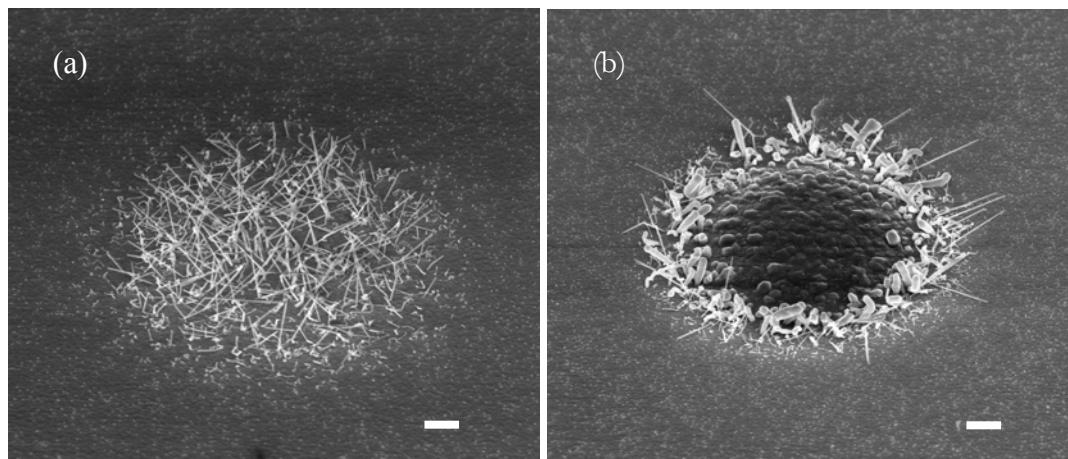


Figure 4-2. Scanning electron microscope (SEM) image of SiNWs grown by indirect (a) and direct (b) heating of catalysts under far field focused laser beam. The scale bars in the figures are 1 μm .

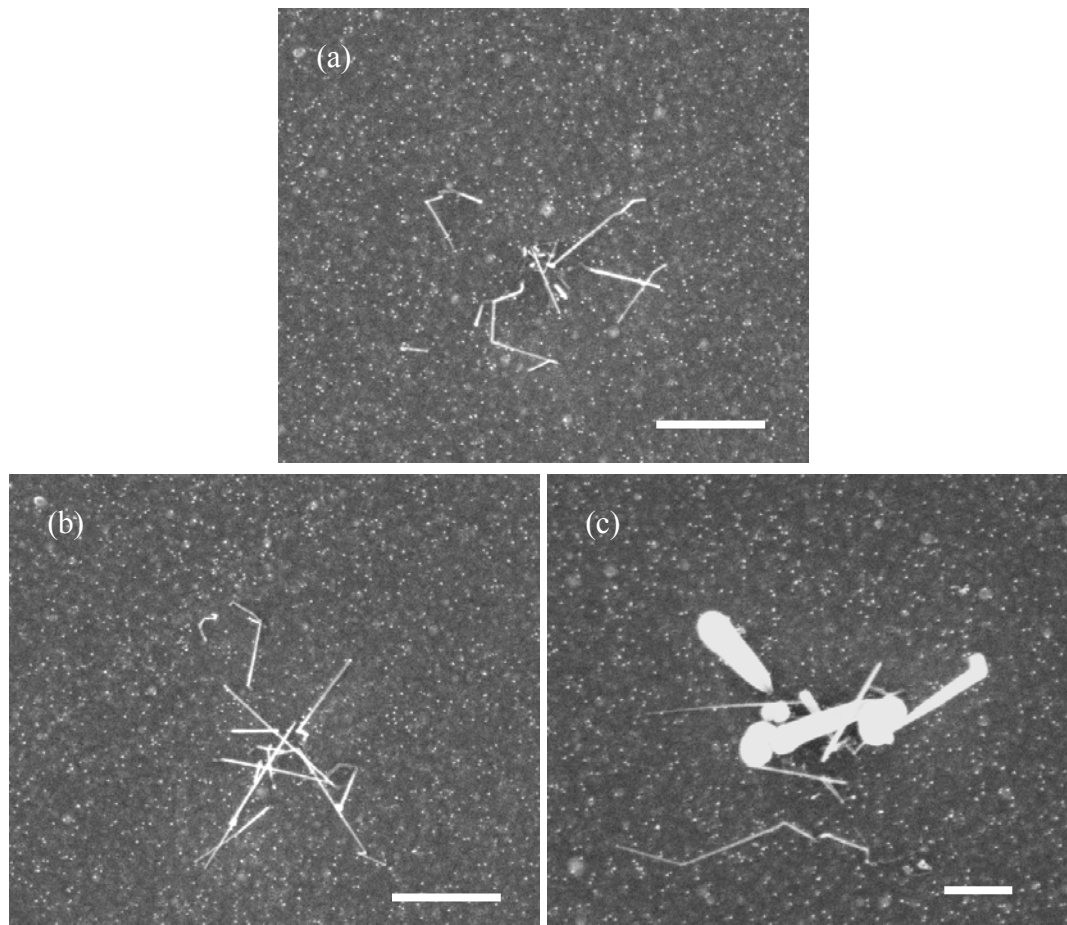


Figure 4-3. Scanning electron microscope (SEM) image of SiNWs grown by minimal direct heating of catalysts under far-field focused film-side laser illumination with assistance of substrate-side laser illumination (72 mW). Film-side laser is illuminated at power of 2 mW for 30 s (a), 3 mW for 20 s (b) , and 3 mW for 30 s (c), respectively. The scale bars in the figures are 1 μm .

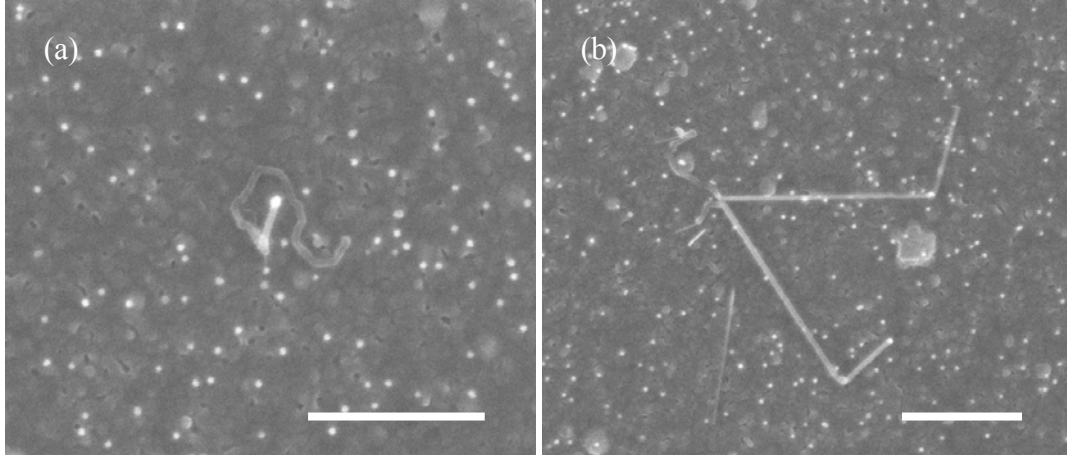


Figure 4-4. Scanning electron microscope (SEM) image of SiNWs grown by minimal direct heating of catalysts under near-field focused film-side laser illumination with assistance of substrate-side laser illumination (72 mW). Film-side laser is illuminated at power of 3 mW for 30 s (a) and 4 mW for 20 s (b), respectively. The scale bars in the figures are 1 μm .

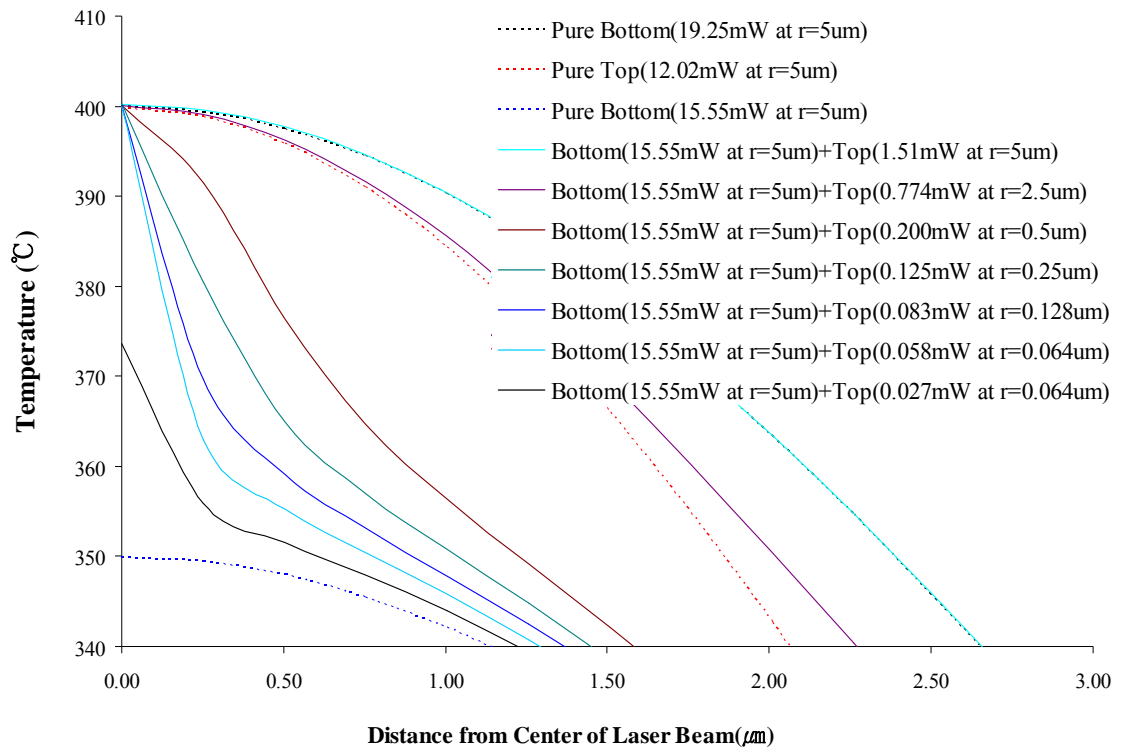


Figure 4-5. Calculated lateral temperature profiles at top surface of a-Si film in the center of the laser spot with different film-side laser illumination beam size coupled with supportive substrate-side laser local heating for local heating of the top surface by 400 °C .

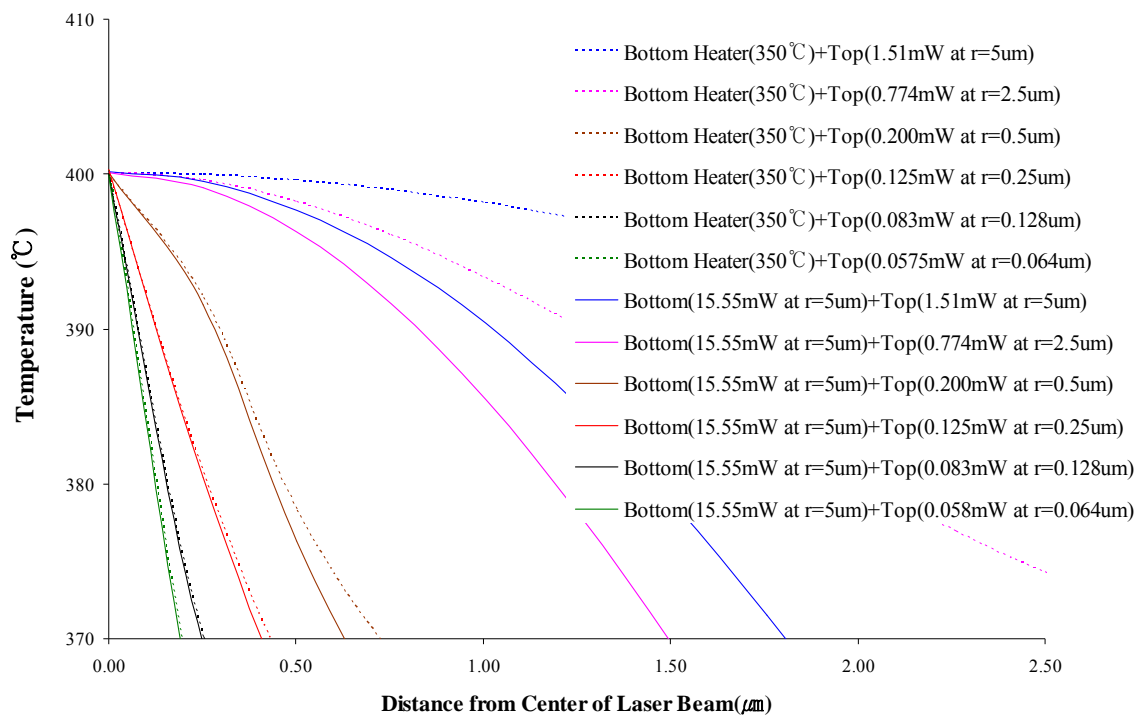


Figure 4-6. Calculated lateral temperature profiles at top surface of a-Si film in the center of the laser spot with different film-side laser illumination beam size coupled with supportive local substrate heating by substrate-side focused laser illumination and with global substrate heating by substrate heater (350 °C) for heating by 400 °C .

CHAPTER 5

ELECTRICALLY BIASED TIP-ASSISTED GROWTH OF A SINGLE SILICON NANOWIRE

To realize SiNWs-based device, it is necessary to control either the direction of growth or arrangement on existing devices. Among techniques aiming at directing one-dimensional nanostructures growth or organizing carbon nanotubes (CNTs) and silicon nanowires (SiNWs), electric field has been demonstrated as a good method by some research groups. This chapter demonstrates that a single silicon nanowire (SiNW) among randomly distributed gold nanoparticles (AuNPs) can be grown in a controlled direction by employing an electrical biased sharp tip. In addition, the electrostatic force to pull a SiNW from the catalyst is estimated by measuring the deflection of the tip at varied bias voltages.

5.1 Overview

As one-dimensional (1-D) nanostructures such as carbon nanotubes (CNTs) and semiconducting nanowires (NWs) have been a promising material to realize future devices, many studies have been extensively focused on the mechanism of their growth. To realize nanostructures-based devices, however, it is also important to grow them with controlled direction and arrangement. Another strategy is to assemble as-grown nanostructures on an existing platform of the device. Several techniques have been studied to assemble or arrange of as-grown nanostructures to date. Fluid flow induced assembly is convenient, but still faces problems in respect to yield and accuracy. More recently, higher level techniques such as optical or optoelectronic tweezing^{34,35} have been applied, but are not sufficient for allowing high spatial and angular resolution. Electrical bias induced direction control of growth has been also reported.^{93,94,95,96,97,98} Respective studies showed that CNTs or SiNWs respond to DC electrical bias during the growth to exhibit directionality. Since this technique offers an advantage to simultaneously arrange nanowires during the growth, it eventually enables pursuit of one-step processes from growth to assembly. Although the effects of electrical bias on control of the direction are still controversial, they can be explained by two mechanisms of electrostatic force and electric field.

When an external electrical bias is applied to an electrical conductor or semiconductor such as CNT and SiNW, internal charges are split into both ends of the nanostructure. Positive charges attracted to applied negative bias move to the conducting or semiconducting substrate. On the other hand, negative charges are attracted to the external positive bias, and are thus accumulated on the end of the nanowire tip. Since the negative charges on the end of the tip are subject to the external positive bias applied object, the electrostatic force generated can play a role of pulling SiNWs toward the direction of the force. The force magnitude can be described by the scalar form of Coulomb's law. The magnitude of electrostatic force exerted on a charge (q_1) by the presence of a charge (q_2) at a certain distance (r) is

$$F_{21} = k_e \frac{q_1 q_2}{r^2} \quad (1)$$

where k_e as coulomb force constant is related to defined properties of space.

$$k_e = \frac{1}{4\pi\epsilon_0} = 8.9875 \times 10^9 \text{ N} \cdot \text{m}^2 \cdot \text{C}^{-2} \quad (2)$$

The electric field created by a single charge (q_2) at a certain distance (r) is

$$E_{21} = \frac{1}{4\pi\epsilon_0} \frac{q_2}{r^2} \quad (3)$$

From Eq. (1), (2), and (3), the relation between electrostatic force and electric field is established in $F_{21} = q_1 E_{21}$. Therefore, external electrical bias can potentially attract the growth of nanowire and guide the direction of the growth following the electric field. This chapter demonstrates that a single SiNW can be selectively pulled and grown in the controlled direction by employing a DC electrical biased sharp tip. To investigate the force to pull a SiNW in a controlled direction starting right from the catalyst rather than bend grown SiNWs with a certain length, the electrostatic force between the substrate and the tip is estimated by measuring the deflection of the tip in response to bias voltage.

5.2 Experimental Setup

Figure 5-1(a) shows a schematic diagram for controlled growth of a single SiNW by externally biased sharp tip. For the sample, 40 nm colloidal gold nanoparticles (AuNPs) were assembled on 4.5 μm amorphous silicon film sputtered on a fused silica substrate. The sample was enclosed within a vacuum chamber which had two optical windows allowing laser access from the bottom side of the sample and monitoring of the sample by a reflection optical microscope from the film side. Continuous wave (CW) Ar^+ laser radiation at a wavelength of 514.5 nm was focused

in the interface of amorphous silicon film and fused silica substrate by 10X objective lens. Sufficiently thicker film than the optical penetration depth at the laser wavelength (514.5 nm) was selected in order to minimize direct heating of AuNPs and simultaneously guarantee sufficient absorption of laser energy from laser in the film. Laser illumination time was varied in the range of 1–30 s by a mechanical shutter. Laser power was controlled by an attenuator consisting of a half wave plate and a polarizing beam splitter and monitored in real time via the beam reflected out of a polarizing beam splitter. 0.9% SiH₄ diluted in He was introduced into the reaction vacuum chamber at 200 sccm maintaining 6.5 Torr as a partial pressure. A sharp atomic force microscope (AFM) tip (0.01-0.025 Ω-cm, Antimony (n) doped, ESP, Veeco Instruments Inc.) was employed for local electric field generation as shown in Figure 5-1(b). The distance between the top surface of the sample and the AFM tip apex is maintained at 2 μm by the probe beam reflected from the top surface of the tip into a quadratic PSD (positioning sensitive diode). Positive and negative DC electrical bias voltages were applied to the AFM tip and the sample, respectively. The electric potential was fixed at 46 V in total.

5.3 Experimental Results & Discussion

5.3.1. Selective and controlled growth of a single SiNW by an e-biased sharp tip

The SEM images in Figure 5-2 that were taken from different angles, show quite surprisingly that only a single SiNW among the randomly distributed AuNPs is directed at 55° from the surface by the external electrically biased sharp tip (Figure 5-1(b)). Indirect localized heating was provided by laser power of 69 mW for 10 s. Neighboring AuNPs remained intact, although they lied within the heat affected zone. For no external bias at the same laser power and growth time, it has been already shown in my previous experiments that SiNWs at the onset of the apparent growth tend to crawl along the surface of the film when grown on a-Si film without external bias, as shown in Figure 5-3. After a certain elapsed time, SiNWs grow epitaxially in the direction offering the lowest energy. Consequently, the nanowire root segment tends to have orientation different than the stem's. Therefore, this study focuses on controlling the SiNW root orientation during the initial growth stage. It is significantly found by employing the electrically biased sharp tip that the root (extending to about 100 nm from the bottom in Figure 5-2(b)) of the grown SiNW is aligned along the same direction as the rest of the NW. Since AuNPs as catalysts are intrinsically negatively charged, they are electrostatically attracted by a positively biased sharp tip. In addition, since the electric field is enhanced in the nanostructured geometries such

as sharp tip as well as nanoparticles, the electrostatic force is also enhanced in proportion to the electric field, according to Eq.(1) and (3). Therefore, the experimental result indicates that externally biased sharp tip possibly forces the catalyst to be pulled along the direction of the induced field due to enhanced electrostatic force and electric field, resulting in controlled growth of the initial SiNW portion. In fact, once a SiNW starts growing along the controlled direction, it can be easily grown along the same direction due to the epitaxial growth characteristics.

For further investigation on the controlled growth by externally biased tip, a plateau tip of 1.8 μm in diameter was also employed in the experiment as shown in Figure 5-4(a). For the plateau tip, the gap between the plateau and the substrate was also maintained at 2 μm , i.e. the same as for the sharp tip. Although the same electric potential (46 V) was applied as on the sharp tip, resulting in 23 V/ μm of the electric field without considering field enhancement effects, it appears that the biased plateau tip does not impose external bias effect on the controlled growth on SiNWs shorter than 1 μm as shown in Figure 5-4(b). Previous reports have focused on the alignment via bending as-grown SiNWs or CNTs.^{93,94,96} Joselevich *et al.*⁹³ also reported that the alignment of CNTs depends on their diameter as well as the length due to the different torque exerted by external field. Englander *et al.*⁹⁶ demonstrated the electric field assisted growth of SiNWs depending on their length. It is reported in the study that longer SiNWs are more effectively aligned along the directions of electric field (5 V/ μm) while 2-3 μm SiNWs stray from the direction of the same induced field, resulting in random growth orientation. Therefore, it is believed that SiNWs shorter than 1 μm need higher electrostatic potential to be bent and aligned along the electric field than 23 V/ μm as shown in the aforementioned experiment. It is apparent that the electrical field exerted by the biased plateau tip is not of sufficient potential to pull the catalyst and hence align the SiNW root during the synthesis.

5.3.2. Electrostatic force for pulling a SiNW from a gold catalyst.

As shown in the results obtained by using the biased sharp tip and the plateau tip, much higher electrostatic force is required to align a SiNW by pulling the catalyst from the beginning of the synthesis than by bending an as-grown SiNW of a certain length. It is therefore necessary to estimate to what extent the electrostatic force is formed by the tip geometry and affects the controlled growth. Without considering the field enhancement by the catalyst, the electrostatic force between the a-Si substrate and the tip is experimentally calculated by measuring the displacement of the tip with respect to bias voltage and then by employing Hook's law ($F = -k \cdot \delta$).⁹⁹ The gap between them is initially set by 2 μm . Figure 5-5 shows the measured displacement of the sharp tip and the plateau tip at varied bias voltages. The deflections at the bias voltage of 46 V are

measured at 0.63 μm and 1.7 μm for the sharp tip and the plateau tip, respectively. Given by Hook's law, the calculated electrostatic force is by about three times stronger in the case of the plateau tip (340 nN) than for the sharp tip (126 nN). However, since the measured forces ($F_{measured}$) is the averaged electrostatic force ($F_{tip-substrate}$) acting on between the surface area ($\pi \times (0.9 \mu\text{m})^2$ and $2 \times \pi \times (10 \text{nm})^2$ for the plateau tip and the sharp tip, respectively) of the tip facing the substrate and a similar order projected area on the substrate and, not on the catalyst particle. Consequently, it does not necessarily represent the force to pull the catalyst but, rather depends on the tip geometry. In this estimation, the force between the sloped surface of the tip and the substrate is neglected. In case of the sharp tip, where the radius of the catalyst exceeds the radius of curvature of the tip end as shown in Figure 5-6(a), it is simply assumed that the measured force is the electrostatic force acting on the catalyst. On the other hand, since the surface of the plateau tip is much larger than the size of the catalyst as shown in Figure 5-6(b), it is assumed that the projected area of the catalyst onto the surface of the tip is considered.

$$F_{sharp\ tip-np} \sim F_{measured\ (sharp\ tip-substrate)} \quad (4)$$

$$F_{plateau\ tip-np} \sim F_{measured\ (plateau\ tip-substrate)} \times \frac{A_{projection\ area\ from\ a\ catalyst}}{A_{tip\ surface}} \quad (5)$$

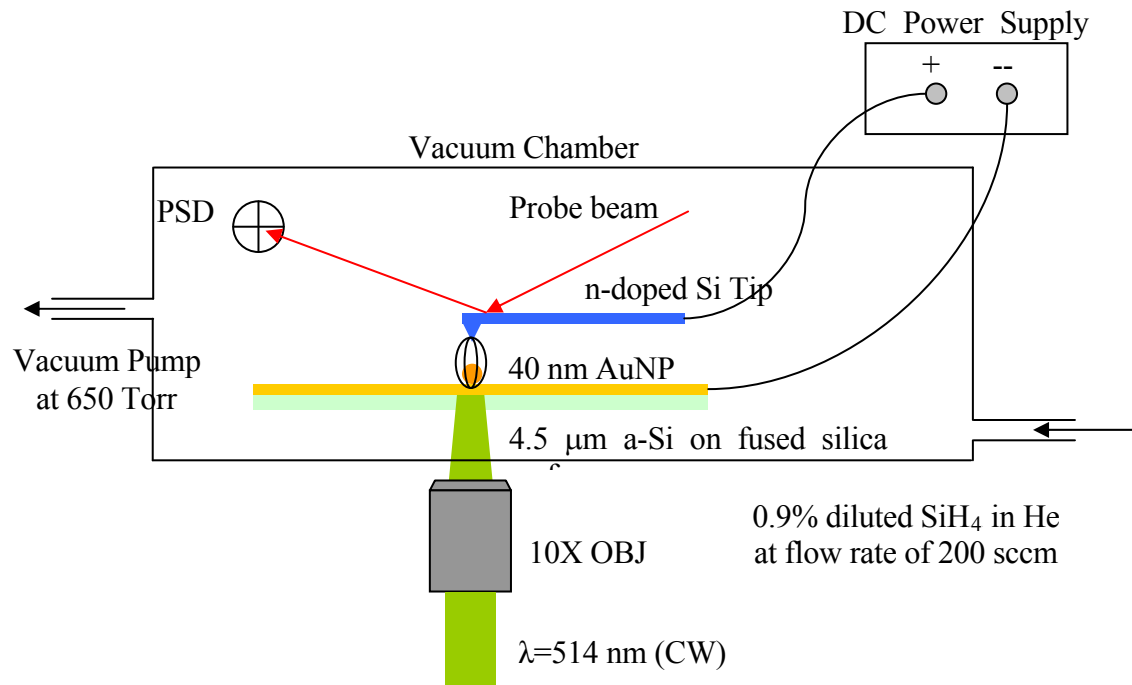
On the basis of Eqs.(4) and (5), it is estimated that $F_{sharp\ tip-np}$ ($\sim 10^2$ nN) is by several orders of magnitude stronger than $F_{plateau\ tip-np}$ ($\sim 10^{-1}$ nN). Although this estimate is certainly approximate, it is argued that a catalyst can be pulled and then grown into a SiNW along the controlled direction due to the highly enhanced electrostatic force ($\sim 10^2$ nN) by a sharp tip. Moreover, if the field enhancement in the gold nanoparticle is considered, the streamline of the effective electric fields would be confined within an even narrower spatial domain extending between the tip apex and the catalyst. A growing SiNW may then be favorably protected from straying away from the direction of the induced field.

5.4 Summary

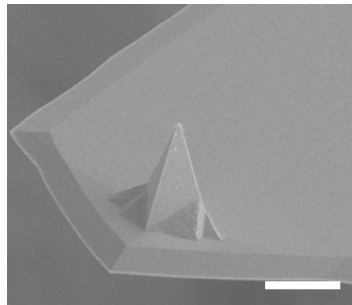
In this chapter, it was demonstrated that highly selective and controlled growth of a single SiNW can be achieved by externally biased sharp tip with. The electric field enhancement by the tip and the catalyst produced greater electrostatic force, resulting in pulling the catalyst along a controlled direction of the induced field and consistently growing a SiNW in the same direction. Experimentally, the electrostatic force, i.e. the force to pull the catalyst by the tip was estimated by measuring the deflection of the tip at varied bias voltages and employing Hook's law. By comparing the electrostatic force

enhanced by a plateau tip with that by a sharp tip, it was also investigated how the geometry of the biased tip can affect the controlled the growth.

FIGURES



(a)



(b)

Figure 5-1. A schematic diagram (a) for controlled growth of SiNW by an electrical biased sharp tip (b) which typically has 10 nm in radius of the tip. The Tip was ESP(0.01-0.025 Ω-cm, Veeco Instruments Inc.) The scale bar in (b) is 10 μm.

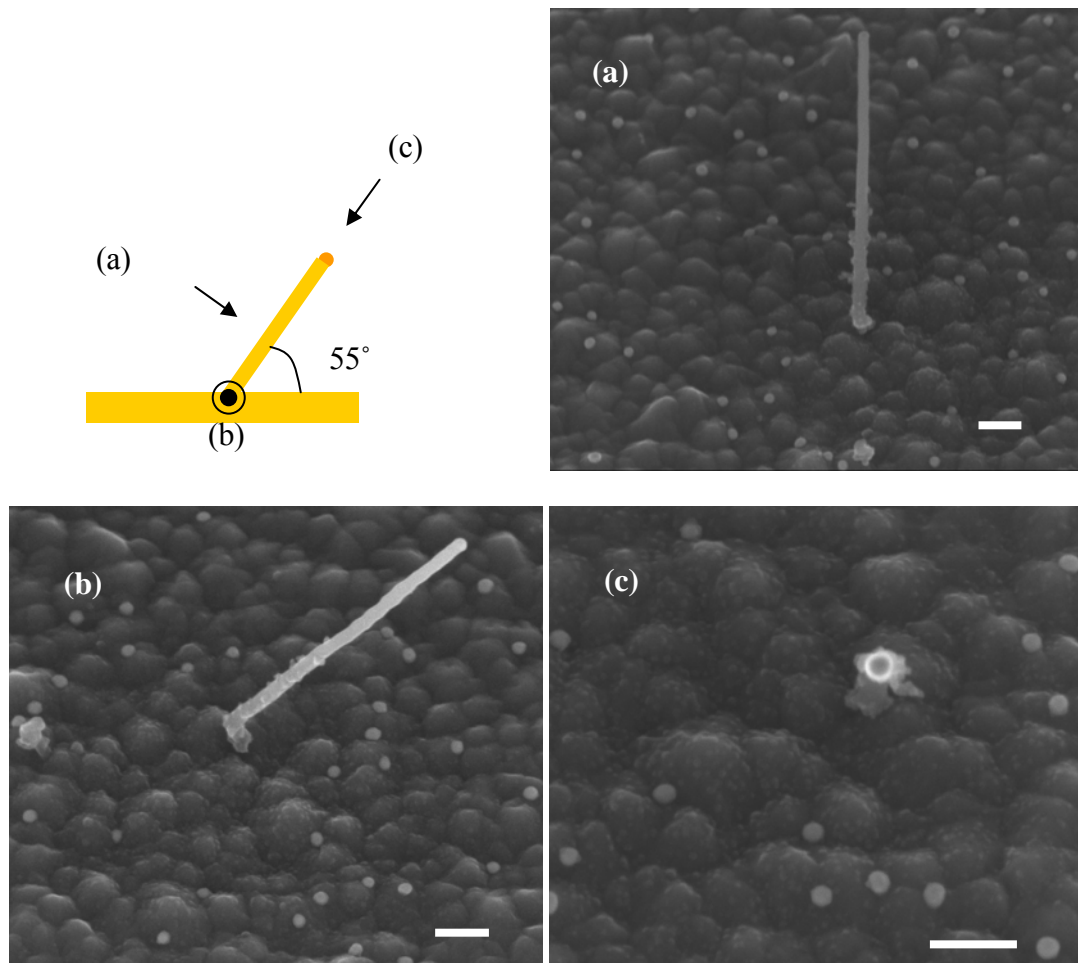


Figure 5-2. A single SiNW among AuNPs randomly distributed on the amorphous silicon substrate AuNPs was directed at 55° by employing DC biased sharp tip of which total voltage was 46 V. Positive and negative biases were applied to the sharp tip and the sample, respectively. A focused laser illuminated in the interface between a-Si film and fused silica substrate heated up the catalysts within heat affected zone to activate the growth of SiNWs. (a), (b), and (c) respectively show an as-grown nanowire at rotation angle of 0° , 90° and 180° with tilted angle of 35° . The bias voltage was 46 V. Laser was illuminated at 69 mW for 10 s. The scale bars in the figures are 200 nm.

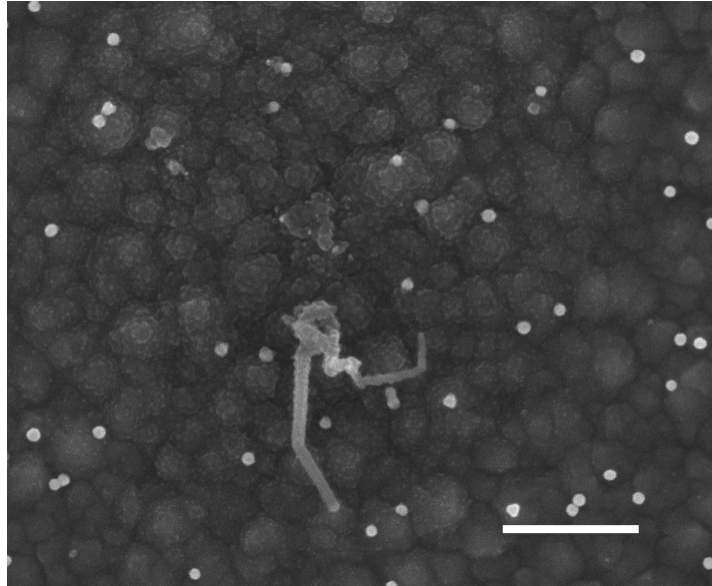


Figure 5-3. SiNWs grown on the amorphous silicon film without an external bias. Laser was illuminated at 69 mW for 10 s. The scale bar in the figure is 500 nm.

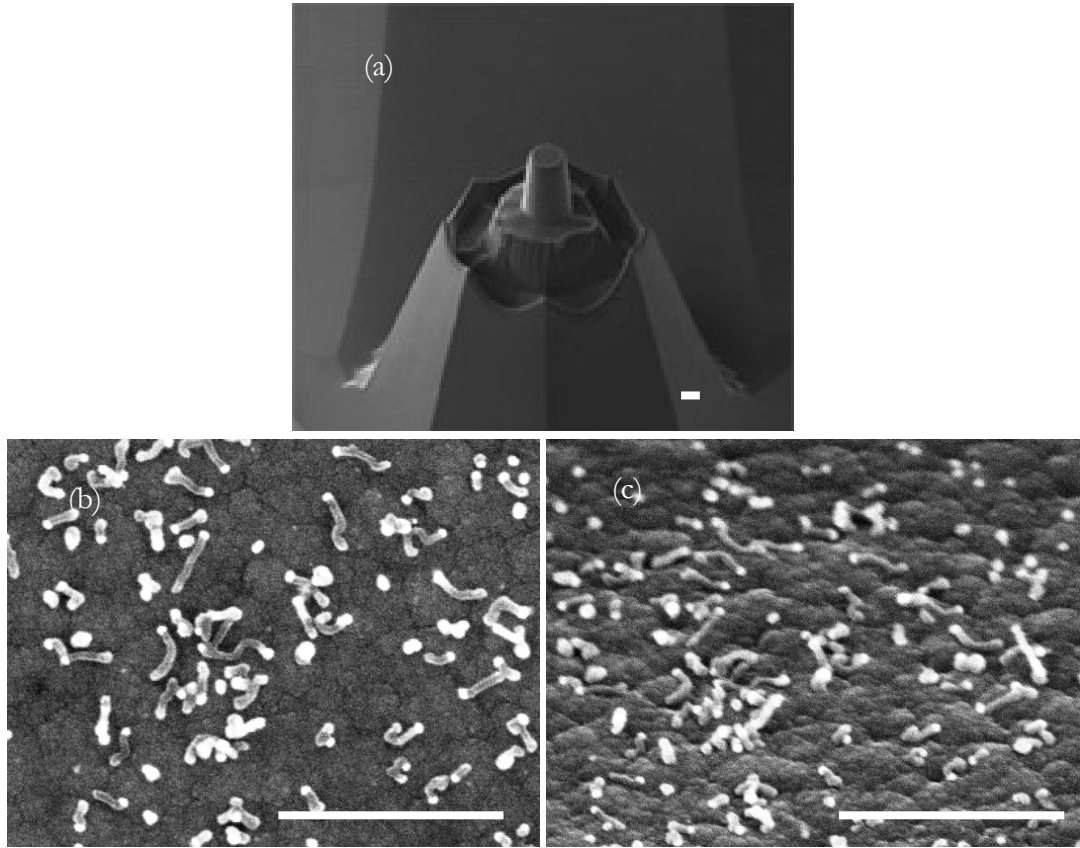


Figure 5-4. SiNWs((b) for top view and (c) for 45° tilted view) grown by the DC positive biased plateau tip (a) which has 1.8 μm in diameter. The tip was PL2-CONTR (NANOSENSORSTM). The bias voltage was 46 V. Laser was illuminated at 72 mW for 10 s. The scale bars in the figures is 1 μm .

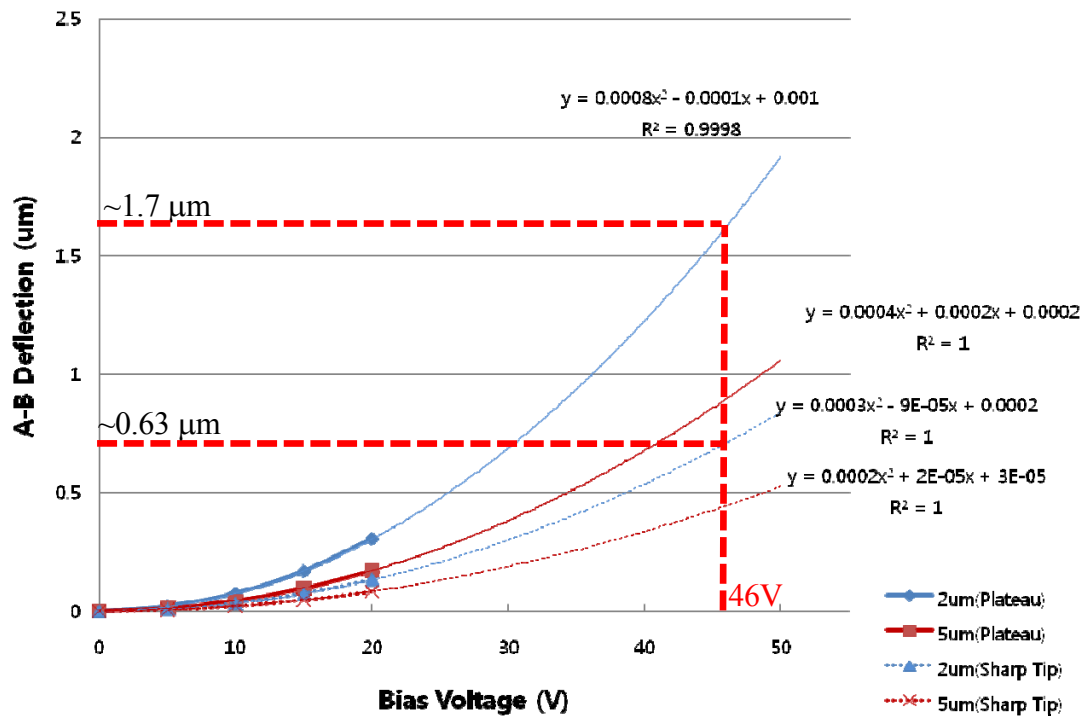


Figure 5-5. Measured deflection of a sharp tip and a plateau tip at varied bias voltages. The sharp tip and the plateau tip was PPP-CONTR ($k = 0.2 \text{ N/m}$, $R_{tip} = 10 \text{ nm}$) and PL2-CONTR ($k = 0.2 \text{ N/m}$, $R_{tip} = 1.8 \text{ }\mu\text{m}$) from NANOSENSORSTM, respectively.

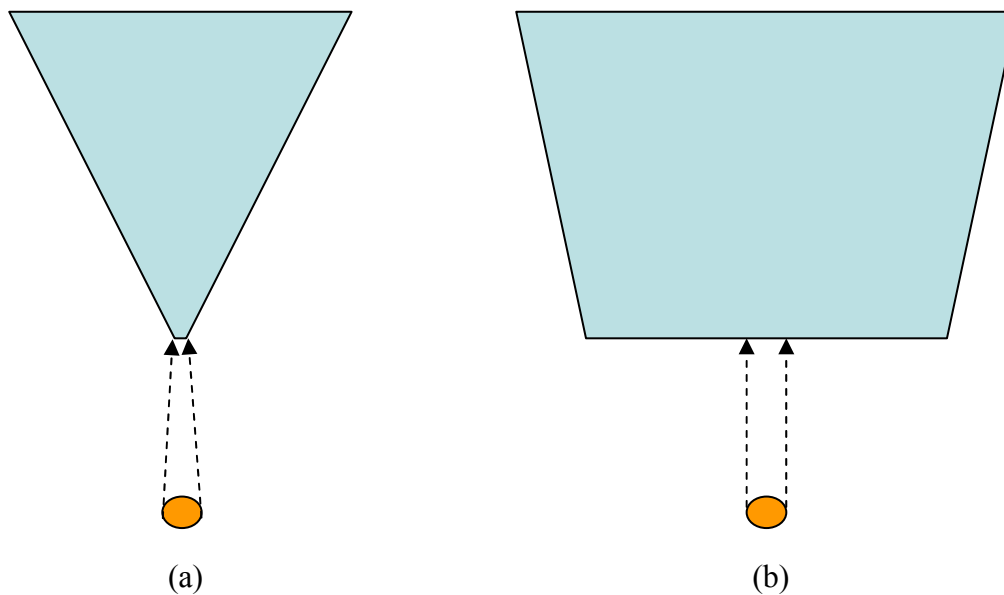


Figure 5-6. Projected area of the catalyst onto the tip depending on its geometry. The field effective area ($2 \times \pi \times (10 \text{ nm})^2$) of the sharp tip (a) is smaller than that of projected area ($\pi \times (20 \text{ nm})^2$) of the catalyst. On the other hand, the surface of the plateau tip ($\pi \times (0.9 \mu\text{m})^2$) is much larger than the size of the catalyst, respectively.

CHAPTER 6

CONCLUSION AND FUTURE DIRECTIONS

In this thesis, the use of laser radiation was introduced for direct and localized growth of silicon nanowires in microscale and nanoscale dimensions, achieved by far-field and near-field optics, respectively. Detailed investigations on the mechanism of laser-assisted growth demonstrated that laser-assisted synthesis is not only a convenient and systematic tool to explore new nanostructure growth mechanisms, but also a highly controllable means for directly growing multiscale nanowires at an arbitrary position accuracy via accessing a wide space of processing parameters. In addition, it was shown that an optical near-field probe- and an electrically biased sharp tip-based technique can synthesize a single silicon nanowire with highly selectivity and controllability. The following are brief summaries for each chapter in this dissertation and an account of future directions.

6.1 Conclusion

In chapter 2, by spatially confining the nanowire growth region via focused laser beam illumination, multi-parametric study was carried out in a single platform by controlling the process conditions such as growth time, laser power, and laser illumination direction. From kinetic analysis, it was shown that laser-assisted growth of SiNWs is thermally activated following Arrhenius like behavior with indirect heating of the catalysts.

In chapter 3, very early stage of growth of SiNWs could be precisely dialed with temporal resolution of 1ms by taking advantage of the faster localized heating capability of laser, compared to conventional furnace process. From the results, the nucleation time decreased in exponential fashion with temperature at the same catalyst size. However, the ratio of the nucleation times corresponding to two different catalyst sizes increased with decreasing temperature possible due to size effect. The activation energy required for the diffusion of silicon through solid Au increased with the catalyst size. Compared to conventional furnace process, shorter nucleation time at early stage as well as faster growth rate in the subsequent growth by 2~3 orders of magnitude showed that three-dimensional diffusion effect of the precursor gas (SiH_4) dominates the nanowire

synthesis. In this respect, it is worth noting that this is the first study to investigate the mechanism of fast growth of SiNWs.

Chapter 4 presented highly selective direct growth of a single silicon nanowire (SiNW) by employing an optical near-field technique. A nanoscale heat source was achieved by a focused laser coupled with an optical near-field probe. Especially, the silicon nitride tip was employed as an optimal near-field probe to protect the probe from heating by laser absorption on its wall. The use of assisting indirect heating could minimize the energy of direct laser illumination over AuNPs, resulting in lowering the local AuNP temperature increase. Consequently, highly selective direct growth of a single SiNW among randomly distributed AuNPs with spacing in nanoscale distance was achieved. It was demonstrated from this study that a laser illumination source confined beyond the diffraction limit in the near field could be a versatile tool for the direct growth of semiconductor NWs at pre-specified area with nanoscale selectivity.

Chapter 5 demonstrated the controlled growth of a single SiNW assisted by electrically biased tip. It was shown that strongly enhanced electrostatic force by a sharp tip has enough potential to pull a catalyst along a specific direction. The study also showed the nanoscale selectivity of the sharp tip provides capability to grow a single SiNW among randomly distributed gold nanoparticles (AuNPs) with spacing in nanoscale distance. Furthermore, to examine the electrostatic force as driving force for the direction control, the deflection of the tip with respect to applied bias voltage was measured as a calibration step.

6.2 Future directions

As shown in this thesis, laser-assisted technique is highly advantageous for localized direct growth of semiconducting nanowires on the prescribed platform. This result can enable multi-nanomaterials synthesis on a single platform that is hard to achieve by conventional furnace scheme. The fabrication of multi-bandgap nanowires on a single platform can be a unique example. Each semiconducting material has a specific bandgap, which can be adjusted by mixing with other matching materials or dopant sources during the synthesis. However, since the selectivity of the available materials or sources is very limited in conventional furnace processes, the resulting nanomaterial bandgap cannot be varied across the wafer. On the other hand, just by switching corresponding gases and controlling their ratio with laser-assisted technique, multi-spectral or -functional nanodevices covering from UV to IR at wavelength can be directly fabricated on a single platform.

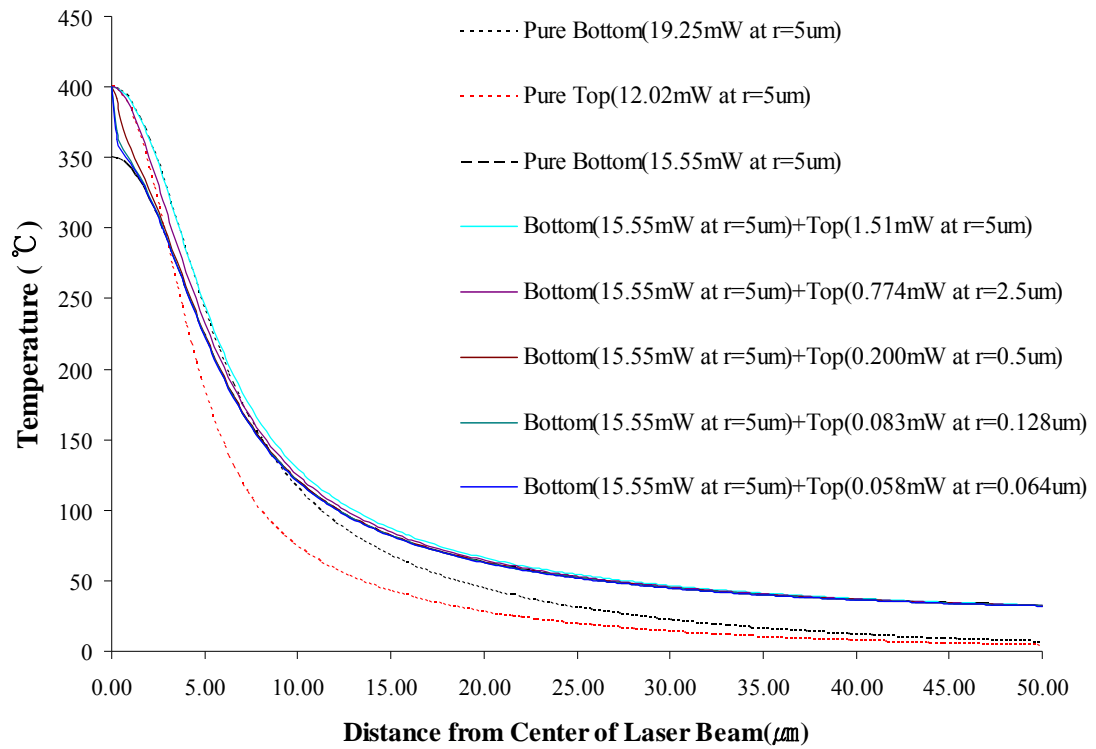
To realize applications, the orientation control of nanowire growth should be more improved. Unlike the amorphous silicon film that was used in this thesis, single crystalline silicon substrate can be considered as a solution for high vertical growth

yield that should be also optimized with processing conditions such as precursor partial pressure and growth temperature. For selective and controlled vertical growth of nanowires, it is also necessary to investigate electrically biased tip assisted growth with systematic experiments.

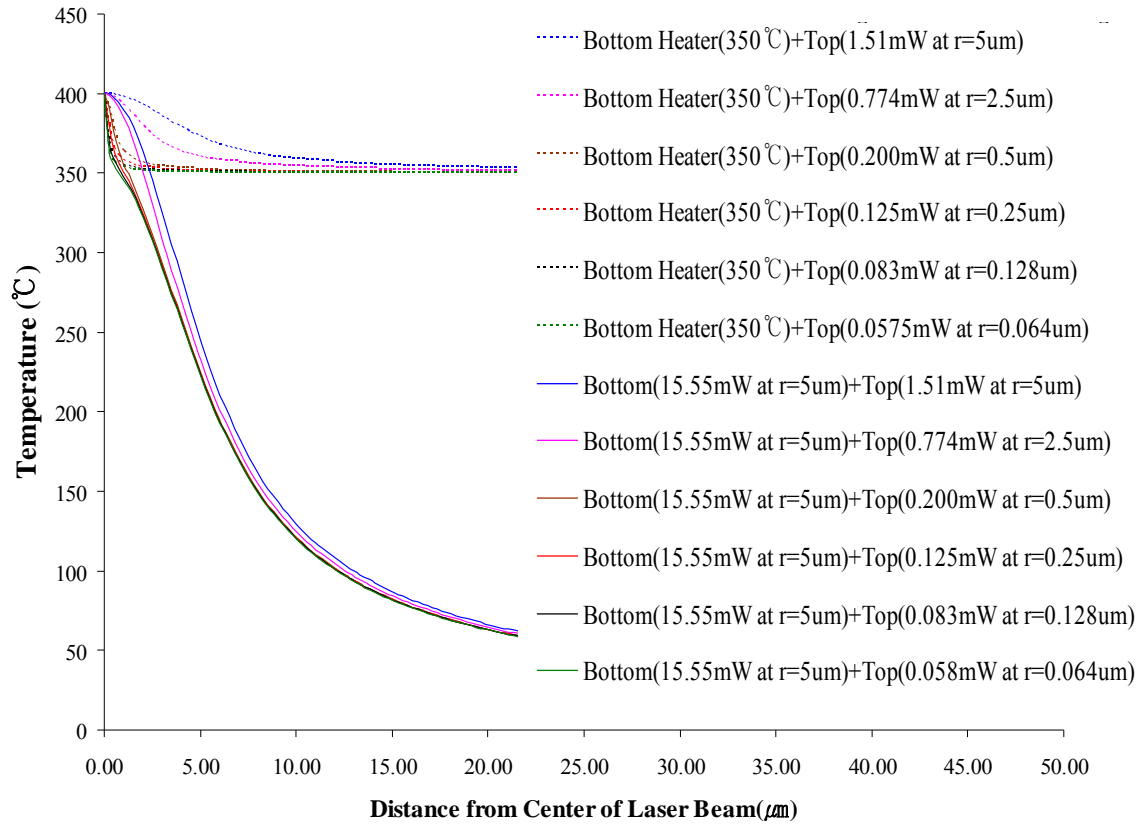
In addition, laser assisted growth of nanowires based on indirect heating of catalysts tends to strongly limit the range of applications. Therefore, different configurations for direct laser illumination based growth should be studied to surpass this limitation, such as employing different laser wavelengths.

APPENDIX

A. Lateral temperature profile in overall distance from the center of the laser spot (extended from Figure 4-5)



B. Lateral temperature profile in overall distance from the center of the laser spot (extended from Figure 4-6)



REFERENCES

- 1 C. J. Barrelet, A. B. Greytak, and C. M. Lieber, "Nanowire photonic circuit
2 elements," *Nano Letters* **4** (10), 1981-1985 (2004).
- 3 M. S. Gudiksen, L. J. Lauhon, J. Wang et al., "Growth of nanowire superlattice
4 structures for nanoscale photonics and electronics," *Nature* **415** (6872), 617-
5 620 (2002).
- 6 Y. Huang, X. F. Duan, and C. M. Lieber, "Nanowires for integrated multicolor
7 nanophotonics," *Small* **1** (1), 142-147 (2005).
- 8 M. Law, D. J. Sirbuly, J. C. Johnson et al., "Nanoribbon waveguides for
9 subwavelength photonics integration," *Science* **305** (5688), 1269-1273 (2004).
- 10 F. Qian, Y. Li, S. Gradecak et al., "Gallium nitride-based nanowire radial
11 heterostructures for nanophotonics," *Nano Letters* **4** (10), 1975-1979 (2004).
- 12 H. Pettersson, J. Tragardh, A. I. Persson et al., "Infrared photodetectors in
13 heterostructure nanowires," *Nano Letters* **6** (2), 229-232 (2006).
- 14 C. Yang, C. J. Barrelet, F. Capasso et al., "Single p-type/intrinsic/n-type
15 silicon nanowires as nanoscale avalanche photodetectors," *Nano Letters* **6** (12),
16 2929-2934 (2006).
- 17 Y. Cui and C. M. Lieber, "Functional nanoscale electronic devices assembled
18 using silicon nanowire building blocks," *Science* **291** (5505), 851-853 (2001).
- 19 Y. Cui, Z. H. Zhong, D. L. Wang et al., "High performance silicon nanowire
20 field effect transistors," *Nano Letters* **3** (2), 149-152 (2003).
- 21 X. F. Duan, Y. Huang, R. Agarwal et al., "Single-nanowire electrically driven
22 lasers," *Nature* **421** (6920), 241-245 (2003).
- 23 X. F. Duan, Y. Huang, Y. Cui et al., "Indium phosphide nanowires as building
24 blocks for nanoscale electronic and optoelectronic devices," *Nature* **409** (6816),
25 66-69 (2001).
- 26 X. F. Duan, Y. Huang, and C. M. Lieber, "Nonvolatile memory and
27 programmable logic from molecule-gated nanowires," *Nano Letters* **2** (5), 487-
28 490 (2002).
- 29 R. S. Friedman, M. C. McAlpine, D. S. Ricketts et al., "High-speed integrated
30 nanowire circuits," *Nature* **434** (7037), 1085-1085 (2005).
- 31 J. Goldberger, A. I. Hochbaum, R. Fan et al., "Silicon vertically integrated
32 nanowire field effect transistors," *Nano Letters* **6** (5), 973-977 (2006).
- 33 H. Haick, P. T. Hurley, A. I. Hochbaum et al., "Electrical characteristics and
34 chemical stability of non-oxidized, methyl-terminated silicon nanowires,"
35 *Journal of the American Chemical Society* **128**, 8990-8991 (2006).
- 36 A. I. Boukai, Y. Bunimovich, J. Tahir-Kheli et al., "Silicon nanowires as
37 efficient thermoelectric materials," *Nature* **451** (7175), 168-171 (2008).

- 17 E. C. Garnett and P. D. Yang, "Silicon nanowire radial p-n junction solar
cells," *Journal of the American Chemical Society* **130** (29), 9224-+ (2008).
- 18 R. R. He and P. D. Yang, "Giant piezoresistance effect in silicon nanowires,"
Nature Nanotechnology **1** (1), 42-46 (2006).
- 19 T. J. Kempa, B. Z. Tian, D. R. Kim et al., "Single and Tandem Axial p-i-n
Nanowire Photovoltaic Devices," *Nano Letters* **8** (10), 3456-3460 (2008).
- 20 K. Q. Peng, X. Wang, and S. T. Lee, "Silicon nanowire array
photoelectrochemical solar cells," *Applied Physics Letters* **92** (16) (2008).
- 21 B. Z. Tian, X. L. Zheng, T. J. Kempa et al., "Coaxial silicon nanowires as solar
cells and nanoelectronic power sources," *Nature* **449**, 885-U888 (2007).
- 22 L. Tsakalakos, J. Balch, J. Fronheiser et al., "Silicon nanowire solar cells,"
Applied Physics Letters **91** (23) (2007).
- 23 C. K. Chan, H. L. Peng, G. Liu et al., "High-performance lithium battery
anodes using silicon nanowires," *Nature Nanotechnology* **3** (1), 31-35 (2008).
- 24 X. Y. Bi, W. L. Wong, W. J. Ji et al., "Development of electrochemical
calcium sensors by using silicon nanowires modified with phosphotyrosine,"
Biosensors & Bioelectronics **23** (10), 1442-1448 (2008).
- 25 Y. L. Bunimovich, Y. S. Shin, W. S. Yeo et al., "Quantitative real-time
measurements of DNA hybridization with alkylated nonoxidized silicon
nanowires in electrolyte solution," *Journal of the American Chemical Society*
128, 16323-16331 (2006).
- 26 W. W. Chen, H. Yao, C. H. Tzang et al., "Silicon nanowires for high-
sensitivity glucose detection," *Applied Physics Letters* **88** (21) (2006).
- 27 J. Hahn and C. M. Lieber, "Direct ultrasensitive electrical detection of DNA
and DNA sequence variations using nanowire nanosensors," *Nano Letters* **4**
(1), 51-54 (2004).
- 28 Z. Li, Y. Chen, X. Li et al., "Sequence-specific label-free DNA sensors based
on silicon nanowires," *Nano Letters* **4** (2), 245-247 (2004).
- 29 E. Stern, J. F. Klemic, D. A. Routenberg et al., "Label-free immunodetection
with CMOS-compatible semiconducting nanowires," *Nature* **445** (7127), 519-
522 (2007).
- 30 W. U. Wang, C. Chen, K. H. Lin et al., "Label-free detection of small-
molecule-protein interactions by using nanowire nanosensors," *Proceedings of
the National Academy of Sciences of the United States of America* **102** (9),
3208-3212 (2005).
- 31 X. L. Feng, R. R. He, P. D. Yang et al., "Very high frequency silicon nanowire
electromechanical resonators," *Nano Letters* **7** (7), 1953-1959 (2007).
- 32 R. R. He, X. L. Feng, M. L. Roukes et al., "Self-transducing silicon nanowire
electromechanical systems at room temperature," *Nano Letters* **8** (6), 1756-
1761 (2008).

- 33 R. S. Wagner and W. C. Ellis, "Vapor-Liquid-Solid Mechanism of Single
Crystal Growth (New Method Growth Catalysis from Impurity Whisker
Epitaxial + Large Crystals Si E)," *Applied Physics Letters* **4** (5), 89-& (1964).
- 34 P. J. Pauzauskie, A. Radenovic, E. Trepagnier et al., "Optical trapping and
integration of semiconductor nanowire assemblies in water," *Nature Materials*
5 (2), 97-101 (2006).
- 35 A. Jamshidi, P. J. Pauzauskie, P. J. Schuck et al., "Dynamic manipulation and
separation of individual semiconducting and metallic nanowires," *Nature*
Photonics **2** (2), 85-89 (2008).
- 36 D. A. Boyd, L. Greengard, M. Brongersma et al., "Plasmon-assisted chemical
vapor deposition," *Nano Letters* **6** (11), 2592-2597 (2006).
- 37 L. Y. Cao, D. N. Barsic, A. R. Guichard et al., "Plasmon-assisted local
temperature control to pattern individual semiconductor nanowires and carbon
nanotubes," *Nano Letters* **7** (11), 3523-3527 (2007).
- 38 W. H. Hung, I. K. Hsu, A. Bushmaker et al., "Laser Directed Growth of
Carbon-Based Nanostructures by Plasmon Resonant Chemical Vapor
Deposition," *Nano Letters* **8** (10), 3278-3282 (2008).
- 39 Z. Chen, F. Zhu, Y. Wei et al., "Scanning focused laser activation of carbon
nanotube cathodes for field emission flat panel displays," *Nanotechnology* **19**
(13) (2008).
- 40 J. Shi, Y. F. Lu, K. J. Yi et al., "Direct synthesis of single-walled carbon
nanotubes bridging metal electrodes by laser-assisted chemical vapor
deposition," *Applied Physics Letters* **89** (8) (2006).
- 41 Y. Fujiwara, K. Maehashi, Y. Ohno et al., "Position-controlled growth of
single-walled carbon nanotubes by laser-irradiated chemical vapor deposition,"
Japanese Journal of Applied Physics Part 1-Regular Papers Short Notes &
Review Papers **44** (4A), 1581-1584 (2005).
- 42 J. B. Park, S. H. Jeong, M. S. Jeong et al., "The rapid growth of vertically
aligned carbon nanotubes using laser heating," *Nanotechnology*, 185604
(185607 pp.) (2009).
- 43 A. S. Arico, P. Bruce, B. Scrosati et al., "Nanostructured materials for
advanced energy conversion and storage devices," *Nature Materials* **4** (5), 366-
377 (2005).
- 44 P. J. Pauzauskie and P. Yang, "Nanowire photonics," *Materials Today* **9** (10),
36-45 (2006).
- 45 R. X. Yan, D. Gargas, and P. D. Yang, "Nanowire photonics," *Nature*
Photonics **3** (10), 569-576 (2009).
- 46 Q. Qing, S. K. Pal, B. Z. Tian et al., "Nanowire transistor arrays for mapping
neural circuits in acute brain slices," *Proceedings of the National Academy of*
Sciences of the United States of America **107** (5), 1882-1887 (2010).

- 47 G. F. Zheng, F. Patolsky, Y. Cui et al., "Multiplexed electrical detection of
cancer markers with nanowire sensor arrays," *Nature Biotechnology* **23** (10),
1294-1301 (2005).
- 48 D. Bauerle, P. Irsigler, G. Leyendecker et al., "Ar+ Laser-Induced Chemical
Vapor-Deposition of Si from SiH₄," *Applied Physics Letters* **40** (9), 819-821
(1982).
- 49 D. Bauerle, "Laser Processing and Chemistry," Springer-Verlag **3rd Edn**
(2000).
- 50 D. E. Kotecki and I. P. Herman, "A Real-Time Monte-Carlo Simulation of
Thin-Film Nucleation in Localized-Laser Chemical Vapor-Deposition,"
Journal of Applied Physics **64** (10), 4920-4942 (1988).
- 51 J. Kikkawa, Y. Ohno, and S. Takeda, "Growth rate of silicon nanowires,"
Applied Physics Letters **86** (12), 3 (2005).
- 52 D. J. Hwang, A. Chimmalgi, and C. P. Grigoropoulos, "Ablation of thin metal
films by short-pulsed lasers coupled through near-field scanning optical
microscopy probes," *Journal of Applied Physics* **99** (4) (2006).
- 53 Y. Pauleau and D. Tonneau, "Kinetics and reaction mechanisms of laser-
assisted chemical vapor deposition of polycrystalline silicon dots from silane,"
Journal of Applied Physics **91** (3), 1553-1559 (2002).
- 54 M. F. Modest, "Radiative heat transfer," Academic Press, Boston **2nd Edn.**
(2003).
- 55 V. K. Pustovalov, "Theoretical study of heating of spherical nanoparticle in
media by short laser pulses," *Chemical Physics* **308**, 103-108 (2005).
- 56 N. Misra, Y. Pan, N. W. Cheung et al., "Selective processing of semiconductor
nanowires by polarized visible radiation," *Applied Physics a-Materials Science
& Processing* **90** (2), 219-223 (2008).
- 57 C. P. Grigoropoulos, W. E. Dutcher, and K. E. Barclay, "Radiative Phenomena
in Cw Laser Annealing," *Journal of Heat Transfer-Transactions of the Asme*
113 (3), 657-662 (1991).
- 58 C. P. Grigoropoulos, D. J. Hwang, and A. Chimmalgi, "Nanometer-scale laser
direct-write using near-field optics," *MRS Bull.* **32** (1), 16-22 (2007).
- 59 H. Schmid, M. T. Bjork, J. Knoch et al., "Patterned epitaxial vapor-liquid-solid
growth of silicon nanowires on Si(111) using silane," *Journal of Applied
Physics* **103** (2) (2008).
- 60 J. Westwater, D. P. Gosain, S. Tomiya et al., "Growth of silicon nanowires via
gold/silane vapor-liquid-solid reaction," *Journal of Vacuum Science &
Technology B* **15** (3), 554-557 (1997).
- 61 Yi Cui, L. J. Lauhon, M. S. Gudiksen et al., "Diameter-controlled synthesis of
single-crystal silicon nanowires," *Applied Physics Letters* **78** (15), 2214-2216
(2001).

- 62 B. Kalache, P. R. Cabarrocas, and A. F. Morral, "Observation of incubation
times in the nucleation of silicon nanowires obtained by the vapor-liquid-solid
method," *Japanese Journal of Applied Physics Part 2-Letters & Express Letters*
45 (4-7), L190-L193 (2006).
- 63 D. Bauerle, "Chemical Processing with Lasers," Springer-Verlag (1986).
- 64 S. Kodambaka, J. Tersoff, M. C. Reuter et al., "Diameter-independent kinetics
in the vapor-liquid-solid growth of Si nanowires," *Physical Review Letters* **96**
(9) (2006).
- 65 B. J. Kim, J. Tersoff, S. Kodambaka et al., "Kinetics of Individual Nucleation
Events Observed in Nanoscale Vapor-Liquid-Solid Growth," *Science* **322**
(5904), 1070-1073 (2008).
- 66 T. Kawashima, T. Mizutani, H. Masuda et al., "Initial Stage of Vapor-Liquid-
Solid Growth of Si Nanowires," *Journal of Physical Chemistry C* **112** (44),
17121-17126 (2008).
- 67 S. Hofmann, R. Sharma, C. T. Wirth et al., "Ledge-flow-controlled catalyst
interface dynamics during Si nanowire growth," *Nature Materials* **7** (5), 372-
375 (2008).
- 68 P. Buffat and J. P. Borel, "Size Effect on Melting Temperature of Gold
Particles," *Physical Review A* **13** (6), 2287-2298 (1976).
- 69 M. Wautelet, J. P. Dauchot, and M. Hecq, "Phase diagrams of small particles
of binary systems: a theoretical approach," *Nanotechnology* **11** (1), 6-9 (2000).
- 70 R. Vallee, M. Wautelet, J. P. Dauchot et al., "Size and segregation effects on
the phase diagrams of nanoparticles of binary systems," *Nanotechnology* **12**
(1), 68-74 (2001).
- 71 E. Sutter and P. Sutter, "Phase diagram of nanoscale alloy particles used for
vapor-liquid-solid growth of semiconductor nanowires," *Nano Letters* **8** (2),
411-414 (2008).
- 72 H. Adhikari, A. F. Marshall, C. E. D. Chidsey et al., "Germanium nanowire
epitaxy: Shape and orientation control," *Nano Letters* **6** (2), 318-323 (2006).
- 73 C. Kittel, "Introduction to Solid State Physics," Wiley, 588 (2005).
- 74 E. I. Givargizov, "Fundamental Aspects of Vls Growth," *J. Cryst. Growth* **31**
(DEC), 20-30 (1975).
- 75 F. Dhalluin, P. J. Desre, M. I. Hertog et al., "Critical condition for growth of
silicon nanowires," *Journal of Applied Physics* **102** (9), 5 (2007).
- 76 R. S. Wagner and C. J. Doherty, "Mechanism of Branching and Kinking
During Vls Crystal Growth," *J. Electrochem. Soc.* **115** (1), 93-& (1968).
- 77 Y. Li, F. Qian, J. Xiang et al., "Nanowire electronic and optoelectronic
devices," *Materials Today* **9** (10), 18-27 (2006).
- 78 G. F. Zheng, W. Lu, S. Jin et al., "Synthesis and fabrication of high-
performance n-type silicon nanowire transistors," *Advanced Materials* **16** (21),
1890-+ (2004).

- 79 Y. Ahn, J. Dunning, and J. Park, "Scanning photocurrent imaging and
electronic band studies in silicon nanowire field effect transistors," *Nano
Letters* **5** (7), 1367-1370 (2005).
- 80 V. Schmidt, H. Riel, S. Senz et al., "Realization of a silicon nanowire vertical
surround-gate field-effect transistor," *Small* **2** (1), 85-88 (2006).
- 81 L. X. Mu, W. S. Shi, J. C. Chang et al., "Silicon nanowires-based huorescence
sensor for Cu(II)," *Nano Letters* **8** (1), 104-109 (2008).
- 82 D. R. Kim, C. H. Lee, and X. L. Zheng, "Probing Flow Velocity with Silicon
Nanowire Sensors," *Nano Letters* **9** (5), 1984-1988 (2009).
- 83 E. Garnett and P. D. Yang, "Light Trapping in Silicon Nanowire Solar Cells,"
Nano Letters **10** (3), 1082-1087 (2010).
- 84 M. D. Kelzenberg, D. B. Turner-Evans, B. M. Kayes et al., "Photovoltaic
measurements in single-nanowire silicon solar cells," *Nano Letters* **8** (2), 710-
714 (2008).
- 85 P. Koblinski, D. G. Cahill, A. Bodapati et al., "Limits of localized heating by
electromagnetically excited nanoparticles," *Journal of Applied Physics* **100** (5)
(2006).
- 86 S. A. Maier and H. A. Atwater, "Plasmonics: Localization and guiding of
electromagnetic energy in metal/dielectric structures," *Journal of Applied
Physics* **98** (1) (2005).
- 87 H. F. Hamann, S. I. Woods, and S. H. Sun, "Direct thermal Patterning of self-
assembled nanoparticles," *Nano Letters* **3** (12), 1643-1645 (2003).
- 88 A. Heltzel, S. Theppakuttai, S. C. Chen et al., "Surface plasmon-based
nanopatterning assisted by gold nanospheres," *Nanotechnology* **19** (2) (2008).
- 89 A. D. McFarland and R. P. Van Duyne, "Single silver nanoparticles as real-
time optical sensors with zeptomole sensitivity," *Nano Letters* **3** (8), 1057-
1062 (2003).
- 90 G. Raschke, S. Kowarik, T. Franzl et al., "Biomolecular recognition based on
single gold nanoparticle light scattering," *Nano Letters* **3** (7), 935-938 (2003).
- 91 C. Noguez, "Surface plasmons on metal nanoparticles: The influence of shpae
and physical environment," *Journal of Physical Chemistry C* **111**, 3806-3819
(2007).
- 92 P. K. Jain, K. S. Lee, I. H. El-Sayed et al., "Calculated absorption and
scattering properties of gold nanoparticles of different size, shape, and
composition: Applications in biological imaging and biomedicine," *Journal of
Physical Chemistry B* **110** (14), 7238-7248 (2006).
- 93 E. Joselevich and C. M. Lieber, "Vectorial growth of metallic and
semiconducting single-wall carbon nanotubes," *Nano Letters* **2** (10), 1137-
1141 (2002).

- ⁹⁴ Yuegang Zhang, Chang Aileen, Cao Jien et al., "Electric-field-directed growth of aligned single-walled carbon nanotubes," *Applied Physics Letters* **79** (19), 3155-3157 (2001).
- ⁹⁵ A. Ural, Y. M. Li, and H. J. Dai, "Electric-field-aligned growth of single-walled carbon nanotubes on surfaces," *Applied Physics Letters* **81** (18), 3464-3466 (2002).
- ⁹⁶ O. Englander, D. Christensen, J. Kim et al., "Electric-field assisted growth and self-assembly of intrinsic silicon nanowires," *Nano Letters* **5** (4), 705-708 (2005).
- ⁹⁷ Y. Gao, Y. S. Zhou, W. Xiong et al., "Controlled growth of carbon nanotubes on electrodes under different bias polarity," *Applied Physics Letters* **95** (14) (2009).
- ⁹⁸ Q. L. Bao and C. X. Pan, "Electric field induced growth of well aligned carbon nanotubes from ethanol flames," *Nanotechnology* **17** (4), 1016-1021 (2006).
- ⁹⁹ B. Cappella and G. Dietler, "Force-distance curves by atomic force microscopy," *Surface Science Reports* **34** (1-3), 1-104 (1999).